HEINZ NIXDORF INSTITUT
UNIVERSITÄT PADERBORN

Sigrid Dimce

Channel Characterization in 60 GHz

Master's Thesis in Computer Engineering

9 December 2019

Please cite as:
Sigrid Dimce, "Channel Characterization in 60 GHz," Master's Thesis (Masterarbeit), Heinz Nixdorf Institute, Paderborn University, Germany, December 2019.

Distributed Embedded Systems (CCS Labs)
Heinz Nixdorf Institute, Paderborn University, Germany

Fürstenallee 11 · 33102 Paderborn · Germany

http://www.ccs-labs.org/

Channel Characterization in 60 GHz

Master's Thesis in Computer Engineering

vorgelegt von

Sigrid Dimce

geb. am 10. November 1992
in Tirana

angefertigt in der Fachgruppe

Distributed Embedded Systems
(CCS Labs)

Heinz Nixdorf Institut
Universität Paderborn

Betreuer:	**Muhammad Sohaib Amjad**
Gutachter:	**Falko Dressler**
	Holger Karl
Abgabe der Arbeit:	**9. Dezember 2019**

Erklärung

Ich versichere, dass ich die Arbeit ohne fremde Hilfe und ohne Benutzung anderer als der angegebenen Quellen angefertigt habe und dass die Arbeit in gleicher oder ähnlicher Form noch keiner anderen Prüfungsbehörde vorgelegen hat und von dieser als Teil einer Prüfungsleistung angenommen wurde.
Alle Ausführungen, die wörtlich oder sinngemäß übernommen wurden, sind als solche gekennzeichnet.

Declaration

I declare that the work is entirely my own and was produced with no assistance from third parties.
I certify that the work has not been submitted in the same or any similar form for assessment to any other examining body and all references, direct and indirect, are indicated as such and have been cited accordingly.

(Sigrid Dimce)
Paderborn, 9 December 2019

Abstract

Millimeter Wave (mmWave) communications have been in the focus of the research community, not only due to its advantages but also due to the influence that various factors like the weather variations or vegetation, have on signal propagation. The presence of any kind of precipitation, liquid (rain) or solid (particularly wet snow), in the transmission medium is observed to have a high impact on signal attenuation. In order to estimate the attenuation from these weather variations, fading prediction methods have been developed and standardized. This thesis analyzes the impact of rain and wet snow on the radio links at 60 GHz, using the channel model simulator developed by the NYU WIRELESS (NYUSIM), and the fading prediction methods developed by the International Telecommunication Union (ITU). The implemented prediction methods are integrated into the channel model simulator to analyze the attenuation on the radio links through various simulations. The simulation results show that the influence of rain and wet snow is low at very short communication distances and becomes crucial only when the communication distance increases.

Kurzfassung

Kommunikation im Millimeter Spektrum (mmWave) ist eine mögliche Lösung für die stetig steigenden Anforderungen an kabellose Kommunikation. Die Signalausbreitung in diesem Frequenzbereich hängt stark von Eigenschaften der Umgebung ab, wie beispielsweise den Wetterbedingungen oder von der Vegetation. Insbesondere Niederschlag, sei es Regen oder Schnee tragen stark zur Dämpfung des Signals bei. Um effiziente Kommunikationssystem mit diesen Technologien entwerfen zu können, ist es wichtig, diese Effekte beschreiben zu können. Entsprechende Modelle wurden von der International Telecommunication Union (ITU) standardisiert und definiert. In dieser Arbeit werden diese Modelle in den Kanalsimulator der NYU WIRELESS (NYUSIM) integriert. Darauf basierend führe ich eine Simulationsstudie durch um die Wettereinflüsse auf die Signalausbreitung zu analysieren. Die Ergebnisse zeigen, dass der Effekt bei geringen Distanzen nur klein ist, bei größeren Distanzen die Signalqualität jedoch substantiell beeinträchtigt wird.

Contents

Chapter 1

Introduction

In the last years, the demand for higher communication speed and capacity has been increasing in the wireless network, due to the growth of the data traffic and the number of connected devices in the network. A possible solution to this demand is to move the communication to the unused mmWave frequency band [1]. This spectrum covers a large range of frequencies, from 30–300 GHz, or wavelength in the range from 1–10 mm. In addition to the large bandwidth, the small wavelength enables small antenna element size creating the possibility to pack a larger number of antennas in the same physical dimensions. As a result, a narrow beam can be formed that can be used for various applications [1].

Despite the aforementioned advantages, the communication distance in the mmWave frequency band is limited to short ranges due to the high path loss. The reason behind the high path loss is the very short wavelength, which makes the electromagnetic wave more sensitive to various effects like vegetation, rain or human body, compared to the communication in lower frequencies [2]. The impact that these factors, particularly weather variations, have on the signal propagation has been in the focus of many papers. Several measurement campaigns, conducted to explore the attenuation level from the rain in different frequencies of mmWave band [3]–[5] have shown that rain is an important attenuation factor in radio links. Other studies have shown that apart from rain, wet snow has also a large impact on signal attenuation, which can be even higher than the attenuation from pure rain [6]. However, the measurement campaigns for collecting data on the attenuation from wet snow have been much rarer compared to the case of rain. This is a result of the difficulty in collecting experimental data since the attenuation from the propagation should be divided from the attenuation due to the antenna icing [6].

To estimate the attenuation level in different scenarios, it is necessary to develop and use fading prediction methods. Several fading prediction methods have been developed for estimating the attenuation from rain, but the most well-known model

is the one developed by the ITU. In the case of wet snow, the situation is different, there is only the fading prediction method developed by the ITU [6].

This thesis aims to study the impact of rain and wet snow on signal propagation at 60 GHz using the fading prediction methods proposed by the ITU. The unlicensed 60 GHz frequency band has drawn the attention of the research community due to the extra attenuation in this frequency. The extra attenuation is a result of the absorption from the oxygen molecules in the atmosphere, which reaches a peak value in this frequency and limits the communication to short distances. The limitation to short distances enables higher frequency reuse since a larger number of devices can operate at the same frequency in the same area, compared to links with longer distances.

As a result of the interest shown in communication at 60 GHz, channel models (e.g. METIS [7], MiWEBA [8]) and a few channel model simulators (e.g. QuaDRiGa [9], NYUSIM [10]) have been already developed. After some initial investigation, I have decided to use the NYUSIM channel model simulator developed by the NYU WIRELESS[1], which is extended by the prediction methods, to perform the simulations.

The contributions of this thesis are the following: First, the validation of the channel model simulator is done at 60 GHz. For this step, I use the measurement results, at 60 GHz, published in various papers, recreate the same scenarios in the simulator, and compare the simulation results with the results presented in these works. Then I implement two fading prediction methods, developed by the ITU, that estimate the attenuation from rain and combined rain and wet snow. The methods are integrated into the NYUSIM, and the estimated attenuation values are added to the total path loss computed by the simulator. The simulator as well provides a way to estimate the attenuation from rain. The rain attenuation is computed for different rain intensities, using the simulator model and the results are compared over the attenuation results estimated using the implemented method. For the communication distance ranging from 1–200 m, the implemented method predicts larger attenuation for the same rain intensities and considers in the calculation the polarization type. As a result, the simulator method is replaced by the implemented method, considering as well the fact that the implemented method has been updated over the years. Afterward, I compute the total atmospheric attenuation capturing the effect of dry air (including O_2), water vapor (H_2O), rain and haze. For estimating the total atmospheric attenuation, I use the function provided by the simulator for computing the atmospheric attenuation without the component for the rain attenuation. Then the rain attenuation calculated from the implemented prediction method is added to the total atmospheric attenuation. For the computation, I use real data for the temperature, barometric pressure, humidity, and rain intensity,

[1] `https://wireless.engineering.nyu.edu/home/`

obtained from the weather station at the Paderborn University [2]. The results for three different scenarios show that the total atmospheric attenuation reaches small values for communication distances ranging from 1–200 m. However, it is important to emphasize that the atmospheric attenuation is a function of parameters that can take different values depending on the weather conditions. The attenuation is computed only for three scenarios and the intensity of rain is small. In the end, I run various simulations, and I analyze the results for defining the impact that rain and wet snow have on the radio communication at 60 GHz, over short and long distances.

The rest of the thesis is organized as follows. First, Chapter 2 describes related work to the thesis. Then the basic concepts over which the work is established, are presented in Chapter 3. An outline of the channel model simulator that is used along with the simulator validation results is given in Chapter 4. Chapter 5 describes the prediction methods that are used for estimating the attenuation from rain and combined rain and wet snow, together with the implementation details and the validation of the methods. The simulation setup, together with the metrics used for analyzing the attenuation from the atmospheric variations and the results from the simulations are presented in Chapter 6. Finally, Chapter 7 provides a summary of the results and introduces some ideas for further investigation.

[2] http://wetter.uni-paderborn.de/

Chapter 2

Related Work

In recent years, the idea of moving the communication to the mmWave frequency band has drawn high attention of the research community. Various surveys like [1], [2] provide an introduction on the topic of the mmWave by giving a summary and review of the existing literature. Besides listing the main characteristics in terms of the communication layers, existing channel models, antenna constructions, etc, these works identify at the same time, some of the present constraints and possible future work.

One of the frequencies in the mmWave band, proposed by many researchers, as suitable for communication, is the 60 GHz frequency. Along with the other frequencies in this band, the 60 GHz frequency is associated with several advantages. First, as mentioned in [1], [2], it solves the main issue of the existing technologies, which is the limited wireless spectrum. Moving to a high carrier frequency leads directly to wide bandwidth for transmission. Secondly, the very small wavelength enables small antenna element size, offering the possibility for a larger number of antenna elements to be packed in the same physical antenna, forming, as a result, a narrow beam which is a requirement for different applications [2].

In spite of these advantages, the communication distance at 60 GHz is limited to very short ranges due to the high path loss. According to [2], the electromagnetic wave at 60 GHz, due to the very small wavelength, is more sensitive to effects like material penetration, rain, vegetation or human body, compared to the lower frequencies.

Besides these effects, the 60 GHz frequency is characterized by an extra attenuation factor coming from the atmospheric gases, especially oxygen molecules. The attenuation from the oxygen molecules reaches the peak in this frequency with values sometimes hitting 15 dB/km [2].

Considering the aforementioned factors, before the actual design of a wireless system, it is important to study the propagation characteristics using a channel

model. Accurate modeling of the radio channel is crucial and needs to be done based on real measurements.

The 60 GHz frequency has drawn the attention of the researches even many years ago, like in [11], where measurements are done in the outdoors and indoors scenarios using omnidirectional and directional antennas, which were static during the measurements. The purpose of the measurements was to explore the effect of the location on the frequency fading and use the results for the design of a Orthogonal Frequency Division Multiplex (OFDM) system.

Many other measurement campaigns are conducted in the last years, like the ones presented in [8], [12], [13]. The measurements are done in Berlin, focusing on the study of the radio channel in a busy urban environment, considering both the scenarios, for a static and mobile receiver. The radio channel has been studied by computing different metrics. The measurement data in [13] are analyzed with a focus on the Power Delay Profile (PDP) for both the static and the mobility scenarios. The paper also studies the impact of the human body shadowing, or in other words, the attenuation due to the presence of the pedestrian, temporarily fully blocking the Line of Sight (LOS) path between the transmitter and receiver.

The measurement data, presented in [12], are analyzed focusing on the path loss and the Delay Spread (DS) metrics. A Ray Tracing (RT) tool is used for recreating the same environments, and the results predicted by this simulator are compared to the measurement results.

The other measurement results presented in [8] are used for developing a quasi-deterministic and a link-level-focused channel model. This channel model has been developed as part of the Millimeter-Wave Evolution for Backhaul and Access (MiWEBA) project. The purpose of the project is to study the outdoor mobile links for very small cellular cells, with a radius in the range of several hundred meters. Besides, other channel models have been developed and standardized for capturing the behavior of the radio channel at 60 GHz. A possible classification of the channel models along with the history of the evolution of the mmWave wireless channel models is given in [2].

At the same time, a few channel model simulators (e.g. QuaDRiGa [9], NYUSIM [10]) have been already developed at 60 GHz. QUAsi Deterministic RadIo channel GenerAtor (QuaDRiGa) is an open-source channel model simulator implemented in MATLAB using an object-oriented framework [9]. The simulator captures user mobility and provides the time evolution of the channel coefficients according to the receiver position.

Similarly, the NYUSIM is an open-source channel model simulator implemented in MATLAB. This simulator offers two models, the drop based model, for the scenario when the receiver is static and the spatial consistency model, capturing the receiver mobility [14]. Both the simulators are based on the concept of the clusters, even

though, the definition of this concept is different in each case. According to [10], the number of clusters defined in the NYUSIM has been extracted from the real measurements and is more realistic in the prediction of spectral efficiency compared to some other models, which use a large number of time clusters.

As already mentioned, the communication in the mmWave, including the 60 GHz frequency, is affected by some extra factors due to the very small wavelength. Consequently, a very high effort has been put in studying, conducting measuring campaigns and standardizing methods for predicting the attenuation of the transmitted signal from these factors. Especially the impact of atmospheric variations like rain and wet snow has been the main topic of several research papers [4], [6], [15]–[17]. The measurements presented in these works have been conducted over several years, and the attenuation results are compared over the predicted values estimated using methods standardized by the ITU [18].

In terms of the fading prediction methods, the two most important methods for estimating the attenuation from rain are the ones developed by Crane and the ITU. According to [19] the attenuation from rain is a function of the rain intensity, drop size and shape, and the volume density of the raindrops. Considering that only the rain intensity can be measured, most of the prediction methods, including the mentioned methods, estimate the attenuation based on the rain intensity. Besides the intensity, for computing the attenuation, these methods make use of the regression coefficients, which are a function of the operating frequency. The methods share the same regression coefficients but use different equations for computing the attenuation from rain [19]. Furthermore, both methods divide the world into rain regions, which can be used to determine the rain intensity for the calculations. Even though the concept is the same for both methods, the regions do not correspond with each other [19]. Another difference between these two methods is that the method developed from the ITU has been updated over the years in order to improve the predicted attenuation values.

In the case of the wet snow, the situation is different. Due to the difficulty in collecting real data, there is only the method developed by the ITU for estimating the attenuation from the combined rain and wet snow, described in [18], which has been evolved in the latest standard version [20]. Although much research has shown that the attenuation caused by the wet snow is larger than the attenuation caused by rain, less work is done in developing prediction methods to estimate this attenuation. The reason behind this slow progress is the complication in collecting experimental data since the propagation attenuation should be divided from the attenuation caused by the antenna icing [6].

The impact of these atmospheric variations is crucial especially in the parts of the world like the tropical or the equatorial regions that are characterized by very strong rainfalls [4], or the Nordic countries where the presence of snow is

important [6], [16], [17]. Anyway, the high difficulty in collecting data, especially from the presence of snow, leaves space for further studies and improvements of the standardized fading prediction methods.

In conclusion, communication at 60 GHz is sensible to a large number of factors, due to the small wavelength [2]. Many measurement campaigns have been conducted in the last years to model the radio channel and to study in detail the effect of various factors. The topic of the attenuation from the atmospheric variations, like rain and snow, has specifically attracted high attention. As a result, methods have been standardized for predicting the attenuation from these factors and at the same time, measurements are conducted for validating these methods according to different local climates [4], [16], [17].

In this thesis, the fading prediction methods developed by the ITU are implemented to estimate the attenuation from the presence of rain and wet snow in the transmission medium. These standard methods are integrated into the NYUSIM for analyzing the impact of rain and wet snow on the radio link at 60 GHz. Even though the simulator provides a function for computing the attenuation from the atmospheric variations, including rain, this component is replaced and compared with the implemented standard method. The total atmospheric attenuation is computed using the function provided by the simulator for estimating the atmospheric attenuation, and the rain attenuation calculated from the implemented prediction method. For the computation are used real data for the temperature, humidity, barometric pressure, and rain intensity, taken from the weather station at the Paderborn University. Furthermore, the channel model simulator is validated at 60 GHz, comparing the simulation results with the results published in [8], [12], [13] for the same scenarios.

Chapter 3

Fundamentals

This chapter describes the basic concepts over which this work is established. First, the attenuation from the gaseous molecules is presented together with the main characteristics of rain and snow precipitations. Then, it is discussed the importance of fading prediction methods and a form of classification of these methods. In the end, a classification and a brief description of the wireless channel models are provided, along with some existing channel models at 60 GHz.

3.1 Atmospheric Attenuation

The communication links carry various kinds of information and based on the application, some information can be of high importance. For these scenarios, the communication links are required to be characterized by high availability and reliability [6]. These requirements must be fulfilled despite the conditions under which the links are operating. In such circumstances before designing the wireless communication system, it is important to identify the main components that contribute to the total path loss.

In addition to the free space path loss and shadowing, the atmosphere has a large impact on signal propagation, especially in mmWave. During the propagation in the atmosphere, the electromagnetic signal is attenuated by the gaseous molecules of oxygen and water. This attenuation can not be neglected especially at 60 GHz, where the absorption from the oxygen molecules reaches a peak value. As explained in [21], this attenuation comes as a result of the absorption band created by the broadened and overlap of the spectral lines of oxygen from the atmospheric pressure near the ground. The attenuation due to oxygen can reach values in the range of 15 dB/km, yet, it is important to mention that the intensity of attenuation is a function of various factors like temperature, barometric pressure, rain intensity and humidity.

On the other hand, the water molecules do not have a high impact in signal attenuation in normal conditions (atmospheric pressure: 1 atm, water vapor density: 7.5 g/cm^3), but once the precipitations are formed, liquid (rain) or solid (snow), they can further attenuate the signal. Weather variations (like rain and snow) have a crucial effect in signal attenuation at 60 GHz because the size of the raindrop or snowflake is in the order of the wavelength.

The following sections provide a short description of the characteristics of rain and snow and the effect on the electromagnetic wave propagation.

3.2 Rain

According to the meteorologists [22], rain is a liquid form of precipitation with drop diameter being equal or larger than 0.5 mm. The liquid falling precipitation with a drop diameter smaller than 0.5 mm is called drizzle and is characterized by a low falling rate due to this small size.

As mentioned in [22], the raindrops reaching the surface of the earth rarely have a diameter larger than 6 mm. This comes as a result of the increasing instability as they get larger, and due to the collision between the raindrops, forming afterward smaller drops.

The size of the raindrop is the main factor in defining the drop shape, which differently from what is depicted in literature, it is not tear shape. The shape of the raindrops having a diameter smaller than 2 mm resembles a sphere. Once the diameter increases, the air pressure is larger on the bottom and smaller in the sides, leading to a shape which is flattened on the bottom and wider on the sides.

Rain can be also classified in different ways. Depending on the type of clouds that lead in the formation, the rain can be classified as continuous formed by a layer of clouds covering a large area, or shower, identified to have a short duration and to cover a small area. Another classification divides the rain based on the intensity into light, moderate and heavy, using different threshold values set by the local climate.

The presence of the rain in the transmission medium has a large influence on signal propagation at 60 GHz, due to the comparable size of the raindrop with the corresponding wavelength. As the electromagnetic wave hits the raindrop, two possible effects can occur, scattering and absorption, leading to the attenuation of the wave. This attenuation can be ignored for frequencies below 5GHz [18], but it must be considered for high frequencies, like 60 GHz, where its impact increases rapidly. Furthermore, as a result of the raindrop shape, being flattened on the bottom and wider on the sides, the attenuation caused by the raindrop is higher for the horizontal polarization, compared to the vertical polarization. Due to these reasons,

the impact of the rain on the high frequencies, including 60 GHz, has drawn high attention of the research community.

3.3 Wet Snow

The other form of precipitation, formed by solid water, is snow. One form of snow classification is based on the amount of water present and divides it into two groups: *dry* and *wet* snow. Dry snow is formed from the snowflakes falling through dry air, with low moisture content, creating the appropriate environment for the snowflakes not to stick together, reaching the ground in the form of powdery flakes [22]. On the other hand, the wet snow is formed by the snowflakes falling through air above the freezing temperature with a high content of moist. These conditions are appropriate for the snowflakes to melt, getting covered by a thin layer of water acting as a glue when it is in contact with other snowflakes, producing a larger snowflake.

Many measurement campaigns done during the years have shown that the attenuation from dry snow can be considered negligible [6]. On the contrary, the attenuation from the wet snow, or differently called the melting layer, has shown to reach high values, sometimes even larger than the attenuation from rain [6]. The particles of the melting layer act as they were entirely water but with a larger size, leading as a consequence to a larger attenuation compared to the attenuation from only rain. Once the particles keep melting, the level of water increases, and as a result, due to the instability the drop will get divided into smaller raindrops, and the attenuation decreases to the level of the attenuation from rain [6].

3.4 Fading Prediction Methods

The attenuation from the gaseous molecules and the weather variation is added to the total path loss and can degrade the system performance. One of the possible solutions to overcome this attenuation is to increase the transmission power. However, transmitting with higher unnecessary power can lead to a limitation in terms of spectral re-usability [6] and interference. For this reason, to determine a maximum possible attenuation level, a reasonable solution is to use fading prediction methods.

Referring to [3] the prediction methods can be classified into two categories: *physical* and *empirical* methods. The physical methods try to reproduce the behavior in the attenuation process, and they require to establish a set-up to define the attenuation. These methods are characterized to achieve high-reliability results but at a high complexity cost. On the other hand, the empirical methods are based on the measurements over long periods, in different locations [5], and are characterized by simple mathematical expressions to compute the attenuation. The main disadvan-

tages of these methods are the strong dependence on the measured data and the incapability to involve the physical processes, but due to the calculation simplicity, they have been used more widely.

In my work, I use empirical fading prediction models developed by the International Telecommunication Union-Radiocommunication (ITU-R) sector to explore the attenuation levels from rain and combined rain and wet snow. The ITU is an agency of the United Nations, the purpose of which is to internationally coordinate the telecommunication services. The ITU-R sector is one of the three sectors of ITU, which is focused on radio communication. One of the responsibilities of this sector is to compile Recommendations from radio standardization.

3.5 Channel Model Classification

The design and implementation of channel models is an important step to understand the signal propagation characteristics, before the actual design of wireless systems, and the development of new technologies adapted to it. There are several channel models and from different perspective, they can be grouped in various ways.

A possible classification of the channel models based on the modeling approach is given in [2]. This classification splits the channel models into two major groups: *physical* and *analytical* models as shown in Figure 3.1. The analytical models represent the communication between a transmitter and a receiver mathematically and are mostly used for algorithm development. The physical models, on the other hand, use the electromagnetic characteristics to represent the communication, and depending on the complexity, they can reproduce the channel characteristics at a realistic level. The physical models can be further divided into *deterministic* and *stochastic* models.

The deterministic models are recognized to be very accurate in predicting the channel characteristics in a deterministic way, but with the cost of high computation and modeling complexity [2]. Such models are used in the cases when information for the propagation environment is known (houses, foliage, buildings, etc.) and are very specific to that environment. The most widely used technique in deterministic models is ray-tracing, in which, each multipath component is represented as a ray. Standalone softwares are available for ray-tracing, making the construction of the environment easier. Since the accuracy in predicting the channel parameters is high, this type of model can be used in the cases when the measurement campaigns are expensive or not possible [2].

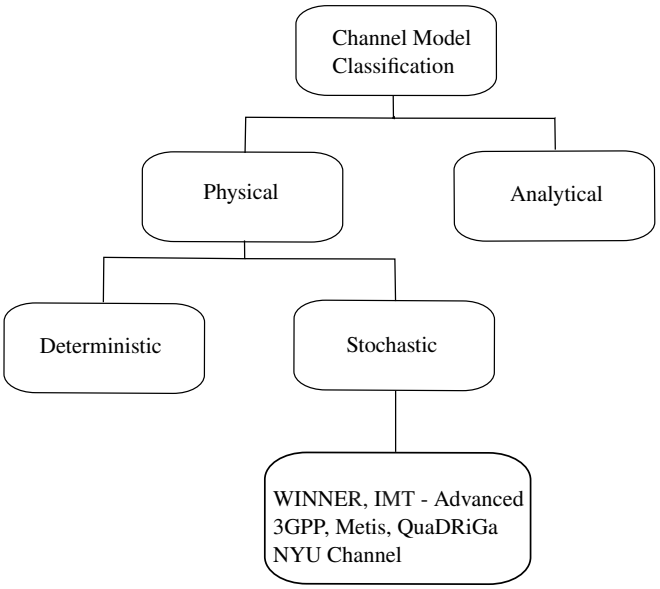

Figure 3.1 – Channel model classification, based on [2].

The stochastic channel models, on the other side, are developed based on the measurements done in different environments and scenarios. Probability density functions are constructed to represent the channel parameters and then used to stochastically calculate the small and large scale fading components. These models are not specific to one environment and are characterized by a lower computation complexity, compared to the deterministic model. The channel model that is used in this work, belongs to this group and a detailed explanation is given in Section 4.1. A short overview of some channel models belonging to this group and modeling the 60 GHz frequency band is given in the following section.

3.6 Existing Channel Models

QuaDRiGa (an acronym for QUAsi Deterministic RadIo channel GenerAtor) is developed by Fraunhofer Heinrich Hertz Institute to model the MIMO radio channel, supporting a wide range of frequencies from 450 MHz to 100 GHz with bandwidth up to 1 GHz. It has an open source implementation in MATLAB using an object-oriented framework. A detailed description of the model is given in [9].

METIS (an acronym for Mobile and wireless communications Enablers for the Twenty-twenty Information Society) has been developed based on measurements done in different environments for different frequencies. As is described in [7], it specifies three models: the map-based model, the stochastic model and the hybrid

model (which is a combination of the two models). Table 8-1 in [7] gives the suitable model which can be used depending on the propagation scenario.

MiWEBA (an acronym for Millimeter-Wave Evolution for Backhaul and Access) uses a 3D quasi-deterministic channel focused on modeling the mmWave outdoor communication channels in 60 GHz based on measurements. As stated in [8] the channel impulse response consists of a few quasi-deterministic strong rays (D-rays) and a number of weak random rays (R-rays), which are combined into clusters.

NYUSIM is an open-source channel model simulator based on MATLAB and developed by the NYU WIRELESS[3]. The NYU WIRELESS is an academic research center focused on the mmWave research. The simulator generates temporal and spatial Channel Impulse Responses (CIR) and is developed based on the measurements conducted in various outdoor environments at frequencies from 28 to 73 GHz [14]. NYUSIM is comprised of the drop based model and the spatial consistency model. The drop based model captures the scenarios when the receiver is static, whereas the spatial consistency model considers the receiver mobility.

Differently from METIS and MiWEBA, the NYUSIM and QuaDRiGa channel models have been also implemented. The channel models in NYUSIM and QuaDRiGa are based on the concept of the clusters, even though the definition is different in each case. The number of clusters generated in the NYUSIM is defined based on the measurements and is smaller compared to the number of clusters generated by the 3rd Generation Partnership Project (3GPP) TR 38.901 Release 15 channel model for frequencies above 6 GHz. Due to the high number of clusters, the 3GPP channel model is more inaccurate in predicting spectral efficiency [14]. Considering that QuaDRiGa is an extension of the WINNER+ and the 3GPP-3D channel models and makes use of a large number of clusters, I have decided to use in the thesis the NYUSIM channel model simulator.

[3] `https://wireless.engineering.nyu.edu/home/`

Chapter 4

Channel Model Simulator and Validation

This chapter introduces the channel model simulator that is used in this thesis, along with the results from the simulator validation at 60 GHz. First, Section 4.1 provides a brief description of the main characteristics of the simulator. Then, Section 4.2 explains the results obtained from the validation and compares them with the results published in the papers used as a reference for the validation.

4.1 Channel Model Simulator

NYUSIM is an open-source channel model simulator, developed by the NYU WIRELESS, to generate temporal and spatial CIR. As explained in [10], the simulator supports a wide range of frequencies (from 500 MHz to 100 GHz), radio frequency bandwidths (from 0 to 800 MHz) and is built upon measurements done in the range of frequencies 28 to 73 GHz in different outdoor environments. A short description of the main characteristics of the simulator is provided in the following subsections.

4.1.1 Path Loss Model

NYUSIM uses the close-in (CI) free space reference distance path loss model with 1 m reference distance and with an extra parameter capturing the effect of the atmospheric variations, expressed as:

$$PL^{CI}(f,d)[dB] = FSPL(f,1m)[dB] + 10n\log_{10}(d) + AT[dB] + \chi_{\delta}^{CI} \qquad (4.1)$$

where $d \geq 1$ m

- f represents the carrier frequency in GHz

- d is the 3-D distance between transmitter T and receiver R
- n represents the path loss exponent (PLE)
- AT term captures the effect of the atmospheric variations
- χ is a zero mean Gaussian random variable with standard deviation sigma, describing the large scale shadowing

The FSPL(f, 1 m) term gives the free space path loss in frequency f, at 1 m distance between the transmitter and receiver, expressed as:

$$FSPL(f, 1\,\text{m})[dB] = 20\log_{10}(\frac{4\pi f \times 10^9}{c}) = 32.4[dB] + 20\log_{10}(f) \tag{4.2}$$

- c represents the speed of light

The FSPL term captures the CI path loss model dependence on frequency and uses a reference distance of $d_0 = 1\,\text{m}$, chosen considering that the communication in mmWave frequencies is characterized by short distance coverage [23]. Based on the results shown in [23], using a reference distance other than 1 m does not lead to a significant difference in the calculation of the other parameters, like shadow fading standard deviation (SF).

The PLE takes different values based on the environment and the scenario in which the communication takes place [14]. In the simulator, the value of the PLE is fixed for the general expression and is recalculated after the effect of the atmospheric variations, cross-polarization, and foliage loss is taken into consideration.

The attenuation term in equation (4.1) is given as:

$$AT[dB] = \alpha[db/m] \times d[m] \tag{4.3}$$

where α is the attenuation factor that captures the collective effect of dry air (including O_2), water vapor (H_2O), rain and haze, and d is the distance between the transmitter and receiver.

Beside CI path loss model, other models have been used to determine the path loss value in mmWave frequency band, like the ABG path loss model adopted by the 3GPP channel model. The models have been compared in [23] and the results show better parameter stability and prediction performance manifested by the CI path loss model over ABG model, in a wide range of frequencies.

4.1.2 Channel Model – Time Clusters and Spatial Lobes

The channel model used in NYUSIM is Statistical Spatial Channel Model (SSCM), based on the concept of time clusters (TC) and spatial lobes (SL). As explained in

[24], TCs consists of multipath components traveling close in time, which can come from different angles during a short window of time. SLs are main directions of arrival (departure) on which multipath components come during a short window of time. This channel model structure is generated based on the measurements and it divides the temporal and spatial statistics. The definition of a cluster in the TCSL channel model differs from the one used in the existing channel models like 3GPP and WINNER model. While in these models a cluster is defined by multipath components traveling along the same propagation path and arriving over a certain Angle of Arrival (AoA) angular spread at the same time, in the TCSL the multipath components belonging to the same TC can come from different angles. The number of clusters is randomly generated in NYUSIM, taking values ranging from 1 to 6, using a uniform distribution. This range of possible number of clusters has been extracted from the measurements and is more realistic in the prediction of spectral efficiency, as mentioned in [10], compared to the Release 14 of 3GPP for frequencies above 6 GHz, where the number of clusters is defined as 12 in LOS scenarios and 19 in Non Line of Sight (NLOS), leading to a large number of simulated mmWave channels and unrealistic spectral efficiency.

4.1.3 Spatial Consistency Model

Most of the statistical channel models are static drop based models, where the subsequent simulation runs give independent CIR [25]. In reality, as mentioned in [26] a user moving in a local area, should be exposed to a similar scattering environment. Using a static drop based model for this scenario is inadequate due to the lack of a necessary continuously update of the temporal and spatial parameters.

To model the user mobility, the NYUSIM has been extended by the feature of spatial consistency. As explained in [26], spatial consistency refers to a similar scattering environment experienced by a user while moving in a local area, causing smooth channel transition. In this way, the NYUSIM has been expanded from a static drop based model, generating independent CIR, to a dynamic model which generates realistic time and distance varying CIR, as the receiver moves in a local area.

Spatial consistency is obtained making use of correlated large scale parameters and time-variant small scale parameters. A 2D grid map, together with an exponential spatial filter, which is applied to independent random values, is used to generate correlated large scale parameters, like shadow fading and LOS/NLOS conditions. The size of the grid is defined by an important parameter called the *correlation distance* reaching values from 10–15 m. The correlation distance represents the concept of the local area and defines a channel segment, within which the channel is highly correlated. Once the receiver moves beyond the correlation distance, the

CIR can be considered independent. The channel segments are connected by using a procedure called cluster birth and death in a way to obtain a smooth transition. Furthermore, the channel segments can be divided into channel snapshots based on the so-called *update distance*. The update distance defines the rate in which the CIR are generated and the small scale parameters are updated for each Multi Path Component (MPC). The small scale parameters consist of power, excess delay, AoA, and Angle of Departure (AoD). Considering that the small scale parameters are time-variant, the update distance is shorter compared to the correlation distance.

A detailed explanation of how the spatially correlated large scale parameters are generated, how the small scale parameters are getting updated in each snapshot, and how the procedure of cluster birth and death is done can be found in [26].

4.2 Channel Model Simulator Validation

This section describes the results that are obtained from the validation of the channel model simulator. For the validation of the simulator are selected a few papers that have done measurements at 60 GHz, in outdoor environments. The same scenarios described in these papers are reproduced in the simulator, and the simulation results are compared with the ones presented in the papers. A common issue that is faced during the validation is the limited amount of information provided for the data collected from the measurements in the corresponding papers. For these cases, the values of some parameters have been roughly estimated from the plots presented in these papers.

The validation is done for both the drop-based and the spatial consistency models, and the results generated by the simulations are presented in the following subsections.

4.2.1 Drop-Based Model Validation

First Validation Scenario – In the first paper, the measurements are done in an empty parking area, surrounded by trees [11]. The transmitter is kept at a fixed location while the receiver is moved along a straight line in a distance range from 3 to 25 m from the transmitter. As described in [11], the purpose of the measurements was to explore the influence of the distance in the frequency fading. The antennas used in the experiment were both omnidirectional and directional and were kept static during the measurements. The resulting plot corresponding to the measurements for this scenario is given in Figure 4.1 and shows the received power as a function of the distance from the transmitter in the log scale, using omnidirectional antennas. According to [11], the value of the received power is averaged over 500 measured points.

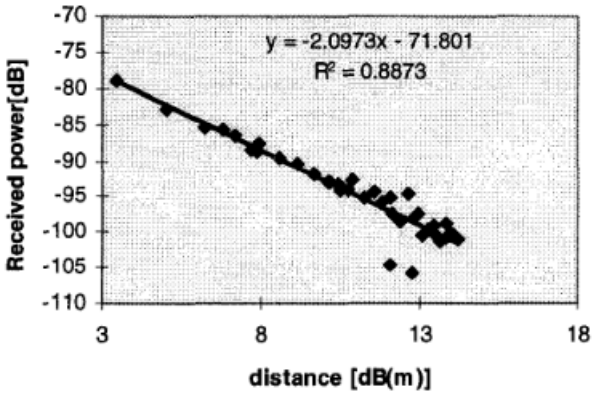

Figure 4.1 – The measured received power as a function of the distance in a log scale, presented in the paper © 1998, IEEE [11].

The relation used in the paper for defining the received power is the following one:

$$10\log_{10}[P_R(d)] = 10\log_{10}[A] - 10\alpha\log_{10}[d] \tag{4.4}$$

where

- P_R is the received power
- d is the distance between the transmitter and the receiver
- A is a constant defined from the transmitted power and the measurement system gain
- α is is the exponent of the power–distance relationship

The two parameters A and α, are estimated in the paper from the received power results using the linear regression technique.

A similar scenario is constructed in the simulator using the parameters provided in the paper. A summary of the parameters used for the simulations is given in Table 4.1.

In my simulations, I give to the PLE the value of the parameter α estimated from the results, and I use the parameter A for computing the transmission power. The value of the transmission power is not given in the paper but is an important input required in the simulations for computing the received power as the difference between the transmission power and the path loss calculated using the Equation 4.1.

Table 4.1 – Summary of the simulation parameter values for the first validation scenario.

Parameter	Values
Frequency	60 GHz
Bandwidth	100 MHz
Scenario	Urban Microcell (UMi)
Condition	LOS
Distance	from 3 to 25 m
Transmission Power	−4.40 dBm
Antenna type (TX and RX)	Omnidirectional
Polarization	Co-Polarization
Half Power Beamwidth (HPBW) in azimuth	120°
Antenna gain	2 dBi
PLE	2.1
SF	4.0

As a result, by using the parameter A as an input to the Friis transmission equation, given in Equation 4.5, I compute the transmission power:

$$P_R = P_T + G_R + G_T + 20\log_{10}(\lambda/4\pi d) \tag{4.5}$$

where

- P_R is the received power, which in this case is replaced by the parameter A
- P_T is the transmission power
- G_R is the receiver antenna gain
- G_T is the transmitter antenna gain
- d is the distance between the transmitter and the receiver
- λ is the wavelength is 60 GHz

The resulting plot from the simulations is presented in Figure 4.2. Each of the points in the resulting plot is obtained as an average of 100 simulation runs. The plot depicts that the received power decreases as the distance between the transmitter and the receiver increases. The behavior of the received power obtained from the simulations, shown in Figure 4.2, is similar to the behavior of the received power obtained during the measurements, presented in Figure 4.1. In the case of the simulation results the received power ranges from −96 dBm to −76 dBm, whereas in the case of the measurement results, the received power ranges from −100 dBm to −79 dBm. Nevertheless, the relative received power is quite similar and the deviation of the results might come since NYUSIM is a stochastic channel model.

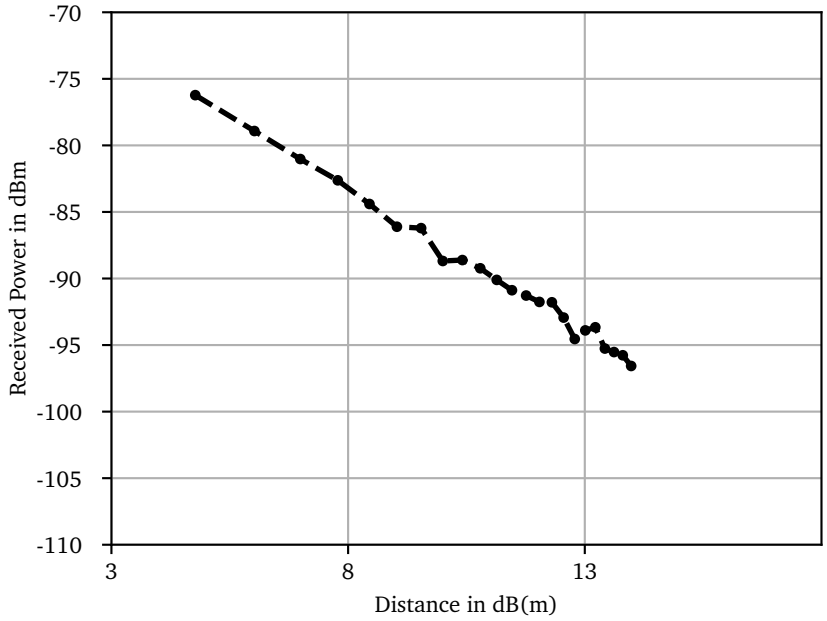

Figure 4.2 – Received power as a function of the distance between the transmitter and the receiver in log scale, obtained from the simulations, for the first validation scenario.

Second Validation Scenario – In the second work, measurements are done in Potsdamer Strasse, Berlin, Germany, which is a street canyon with a width of 51.5 m [13]. The area is a typical urban scenario consisting of buildings from glass and stones, trees, bus stops, etc. Even though the measurements are done for two cases when the receiver is static and mobile, since I am validating the drop based model, I consider only the results for the static receiver. In this scenario, the distance between the transmitter and the receiver is 25 m. The measurement data is analyzed in terms of the CIR for each measurement snapshot. One measurement run takes 50 s and is comprised by 62,500 snapshots, where the temporal separation between two subsequent snapshots is 800 µs. As mentioned in [13], the CIR depicts the propagation delay and the power intensity for each MPC reaching the receiver. The resulting plot for 100 snapshots of CIR, presented in the paper, is given in Figure 4.3.

The same scenario presented in the paper is recreated in the simulator. In order to run the simulations, in addition to the parameters provided by the paper, I had to define some extra parameters required by the simulator. A summary of the parameters used for the simulations is given in Table 4.2.

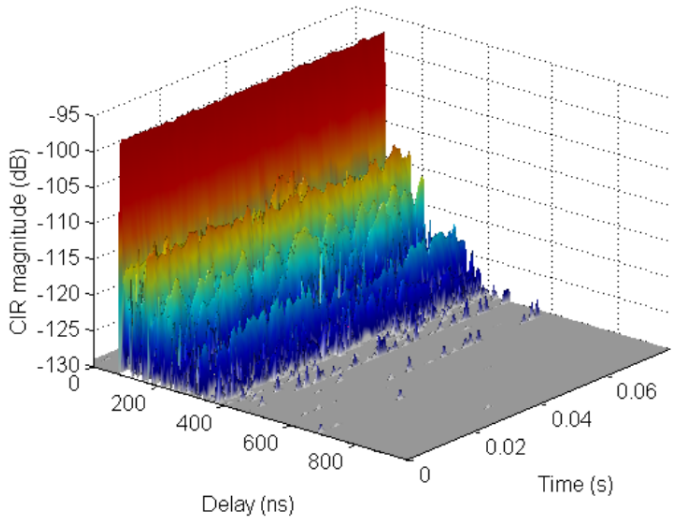

Figure 4.3 – The measurement results of the CIR for the static receiver, presented in the paper © 2014, IEEE [13].

Table 4.2 – Summary of the simulation parameter values for the second validation scenario.

Parameter	Values
Frequency	60 GHz
Bandwidth	250 MHz
Scenario	UMi
Condition	LOS
Distance	25 m
Transmission Power	15 dBm
Antenna Type (TX and RX)	Omnidirectional
Polarization	Linear, Vertical, Co-Polarization
Antenna Gain	2 dBi
PLE	2.36
SF	4.0
Mean Excess Delay	135 ns
Γ	85 ns
Threshold	-130 dBm
Number of Clusters	6
Number of Subpaths	15

Three important parameters that play a crucial role in the simulations, which were not defined in the paper are the followings:

PLE – The value of the PLE is selected based on [27], where measurements are done for the same scenario, using the same devices and parameter values defined in [13]. The PLE is extracted from the measurements using the linear least square (LS) fit and is given in Table I of [27]. In my simulator, this value is used as an input for

the general expression, Equation 4.1 and then is getting recalculated considering the effect of the atmospheric variations.

Mean Excess Delay – The mean excess delay is approximated from Figure 4.3. This value is defined as 135 ns considering the delay of the first MPC and the maximum excess delay. The first MPC comes from the LOS path and has a propagation delay of 83 ns as a result of the distance between the transmitter and receiver. The maximum excess delay is defined as the time delay where the power is reduced by 10 dB. The mean excess delay is computed as the mean of the difference between the maximum excess delay and the time delay of the first MPC.

Γ – The last parameter, Γ, is defined in [24] as the time delay when the cluster power decreases with 37%. This parameter is calculated from Figure 4.3 as 85 ns considering the first two strongest MPCs. The first MPC has a propagation delay of 83 ns, and the strength of the second strongest MPC, obtained after 92 ns, is smaller than by 37%. As a result the value of Γ, is defined as 85 ns.

The resulting plot obtained after the simulation runs is shown in Figure 4.4. The values have been averaged over 10 simulation runs. The power intensity of all multipath components shown in Figure 4.4 is above the threshold -130 dBm, given in Table 4.2. As mentioned before, the first MPC reaches the destination from the LOS path after 83 ns as a result of the distance between the transmitter and the receiver. The other components coming from other directions, propagate through longer paths and as a result, they reach the destination after a longer time with reduced power.

The results obtained from the simulations are compared to the results collected from the measurements in Figure 4.3, in terms of the received power, propagation delay and the number of clusters.

First, in the results presented in Figure 4.3, the clusters can be almost perfectly distinguished over time. One possible reason for this behavior is the short time between the measurement snapshots, which is only 800 μs and the small number of measurement snapshots shown in Figure 4.3 which was only 100. For this reason in my simulations, to obtain the same pattern of the results given in Figure 4.3, I have fixed the number of clusters and the propagation delay to be the same for all the subpaths. Regardless, the number of clusters reaching the destination is different in the two plots. In the case of the measurement results presented in Figure 4.3, the number of clusters is 6, while for the simulation results depicted in Figure 4.4, the number of clusters is 5. In terms of the propagation delay, the last subpaths reach the destination in Figure 4.3 approximately after 700 ns, while in the case of Figure 4.4, the last subpaths reach the destination for the same threshold after 800 ns. While in terms of the received power, the results from the simulations in Figure 4.4 are more optimistic compared to the results from the measurements by sometimes 15 dB.

In conclusion, the behavior of the results collected from the simulations is similar to the results presented in the paper, from the measurements, but with deviations in terms of the number of clusters, received power and the propagation delay as explained above. The reasons for these deviations can be the parameters that are defined approximately from the measurement results and the stochastic nature of the simulator.

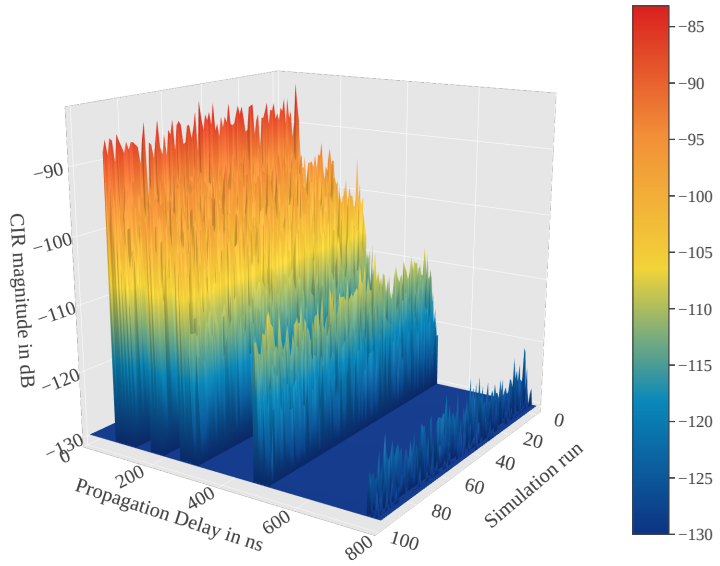

Figure 4.4 – The results obtained from the simulations, showing the received power for each MPC as a function of the propagation delay and simulation run.

Third Validation Scenario – The last scenario for the validation of the static model is an open square city center of octagonal shape, more specifically Leipziger Platz, Berlin, Germany. The area is surrounded by buildings comprised of glass and stone, is covered by grass and some trees [8]. The measurements are done considering the cases when the receiver is mobile and static. Since the purpose is to validate the drop based model, I consider only the results presented for the static receiver.

Measurement results for the static case are presented for two different scenarios or in other words, for two different locations for the transmitter and the receiver. In both cases, the distance between the transmitter and the receiver is 25 m. The collected data is analyzed in terms of the Average Power Delay Profile (APDP), presenting the received power for each multipath component as a function of the propagation delay. The measurement results for the first and the second scenario are given correspondingly in Figure 4.5 and Figure 4.6.

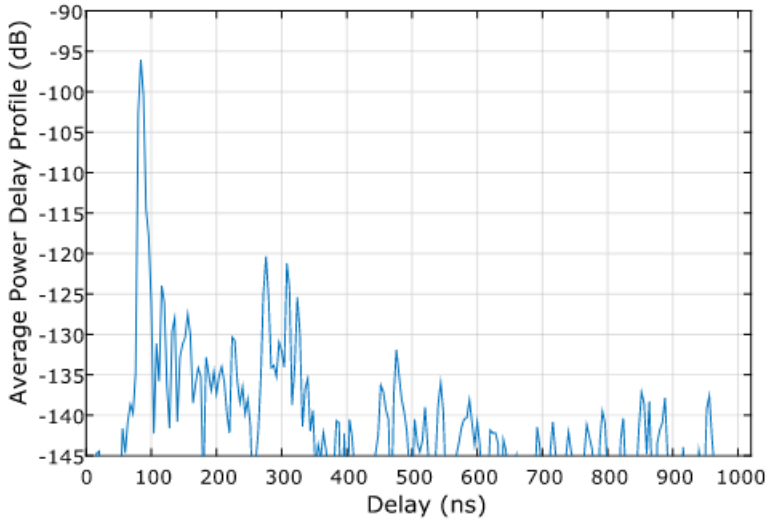

Figure 4.5 – The measured APDP for the first scenario and static receiver presented in the paper [8].

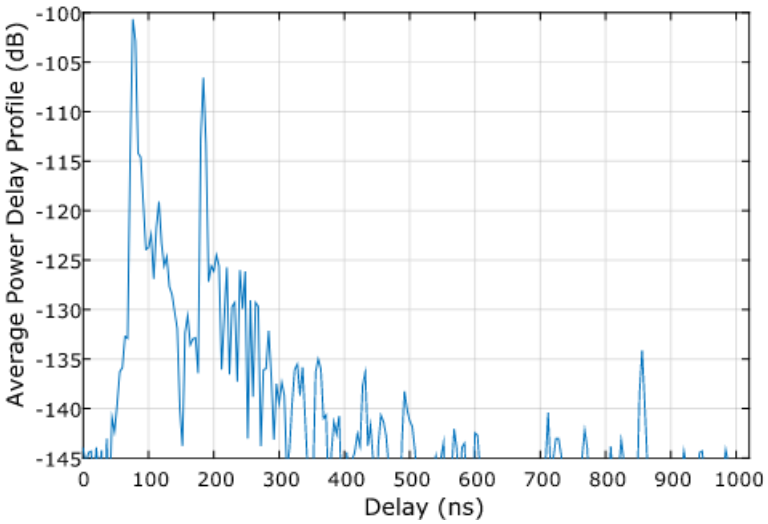

Figure 4.6 – The measured APDP for the second scenario and static receiver presented in the paper [8].

The same scenarios are reproduced in the simulator using the parameter values provided in the paper [8]. In addition to this data, the other missing parameter values, required by the simulator are approximated from Figure 4.5 and Figure 4.6. The parameter values used for the simulations are given in Table 4.3.

For defining the values of the PLE, the mean excess delay, and Γ, I follow the same procedure explained in the previous validation scenario and the values are given in Table 4.3. After running the simulations, the results collected from the simulations,

Table 4.3 – Summary of the simulation parameter values for the third validation scenario.

Parameter	Values
Frequency	60 GHz
Bandwidth	250 MHz
Scenario	Urban Microcell (UMi)
Condition	LOS
Distance	25 m
Transmission Power	15 dBm
Antenna Type (TX and RX)	Omnidirectional
Polarization	Linear, Vertical, Co-Polarization
Antenna Gain	2 dBi
PLE	2.36
SF	4.0
Mean Excess Delay for the fisrt scenario	190 ns
Γ for the first scenario	87 ns
Mean Excess Delay for the second scenario	150 ns
Γ for the second scenario	100 ns
Threshold	-145 dBm
Number of Clusters	6
Number of Subpaths	15

for both the scenarios are given correspondingly in Figure 4.7 and Figure 4.8. The number of the clusters, subpath components, and the propagation delays are fixed, to average the data over multiple simulation runs.

In both cases, the first MPC reaches the destination from the LOS path, with a delay of approximately 83 ns, due to the distance between the transmitter and receiver of 25 m. The other components reach the destination from longer propagation paths, and as a result, the received power of these components is smaller and the propagation delay higher.

Even though the distance between the transmitter and the receiver is the same for both the scenarios, the time when the components of the second cluster will reach the destination is different. This might be a result of the surrounding environment and the distance of the objects surrounding the receiver. This behavior is captured by the mean excess delay parameter, taking different values in both the scenarios, presented in Table 4.3.

In terms of the received power, the results obtained from the simulations, presented in Figure 4.7 and Figure 4.8, are more optimistic compared to the corresponding measurement results shown in Figure 4.5 and Figure 4.6. Nevertheless, the behavior of the received power as a function of the propagation delay is similar between the simulation and the measurement results. The reason for the difference between the results can be the stochastic nature of the channel model simulator.

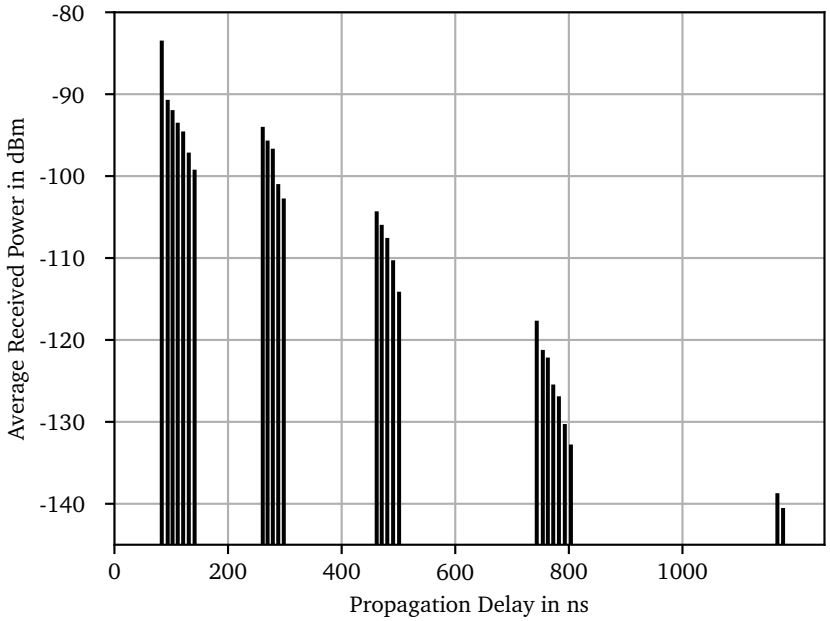

Figure 4.7 – APDP obtained from the simulations for the first scenario.

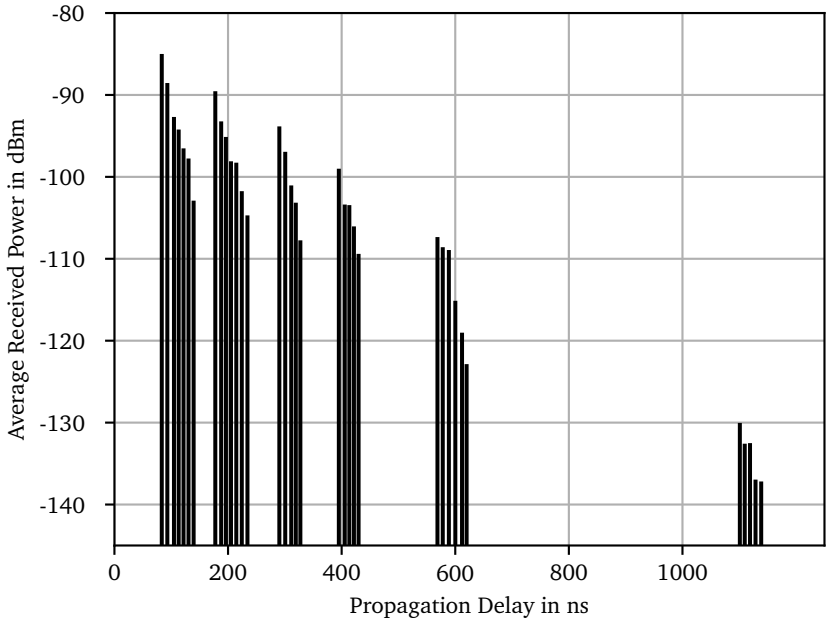

Figure 4.8 – APDP obtained from the simulations for the second scenario.

4.2.2 Spatial Consistency Model

The scenario that I have selected for the validation of the spatial consistency model is the last scenario, already described in the validation of the drop based model. The area is the Leipziger Platz, Berlin, Germany, an open square city center of octagonal shape surrounded by buildings, with trees, covered on grass, as described in [8], [12].

In this case, the receiver is mobile, moving at a speed of 0.5 m/s along a linear track. The distance between the transmitter and the receiver starts from 5 m and reaches the maximum 50 m as a result of the receiver mobility. During the movement, the communication between the transmitter and the receiver is LOS. After collecting the data from the measurements, the path loss and the APDP have been analyzed. The measurement results corresponding to the path loss are shown in Figure 4.9 and the ones related to the APDP are presented in Figure 4.11. The same scenarios are reproduced in the simulator, using the parameters provided in the paper [12], and some extra parameters approximated from the presented measurement results. The parameter values used in the simulations are listed in Table 4.4.

Table 4.4 – Summary of the simulation parameter values for the spatial consistency model.

Parameter	Values
Frequency	60 GHz
Bandwidth	250 MHz
Scenario	Urban Microcell (UMi)
Condition	LOS
Distance	from 5 to 50 m
Transmission Power	15 dBm
Antenna Type (TX and RX)	Omnidirectional
Polarization	Linear, Vertical, Co-Polarization
Antenna Gain	2 dBi
PLE	1.88
SF	1.03
Mean Excess Delay	190 ns
Γ	85 ns
Threshold	-130 dBm
Number of Clusters	6
Number of Subpaths	15
Antenna Height (TX and RX)	3.5 m/ 1.5 m
Receiver speed	0.5 m/s
HPBW in elevation	80°
Direction	0
Correlation distance	10 m
Update Distance	0.4 mm

The value of the update distance is defined 0.4 mm, since in the paper [12] is described that the CIR has been collected every 800 µs corresponding to a receiver movement of 0.4 mm. Since also according to the simulator, the update distance defines the rate at which the CIR are updated, I gave to this parameter the value 0.4 mm.

Furthermore, the values of the PLE and the SF are defined based on the corresponding values derived from the measurements as shown in Table 2 of [12].

Path Loss – After running the simulations, using the parameter values specified in Table 4.4, the path loss metric is analyzed. To compare the data collected from the simulations with the results published in the paper, the values are averaged as described in the paper [12]. The averaging is done over a receiver movement of 1.25 m, corresponding to 3125 collected data points or results.

The results obtained from the simulations are given in Figure 4.10. The plot shows the value of the path loss as a function of the distance between the transmitter and receiver given in the log scale. As expected, the path loss value increases with the distance between the transmitter and receiver. Compared to the results obtained from the measurements presented in Figure 4.9, the plot follows a similar behavior. In terms of the values, the results are similar with a maximum deviation of 5 dB. The reason for this deviation can be the stochastic nature of the simulator.

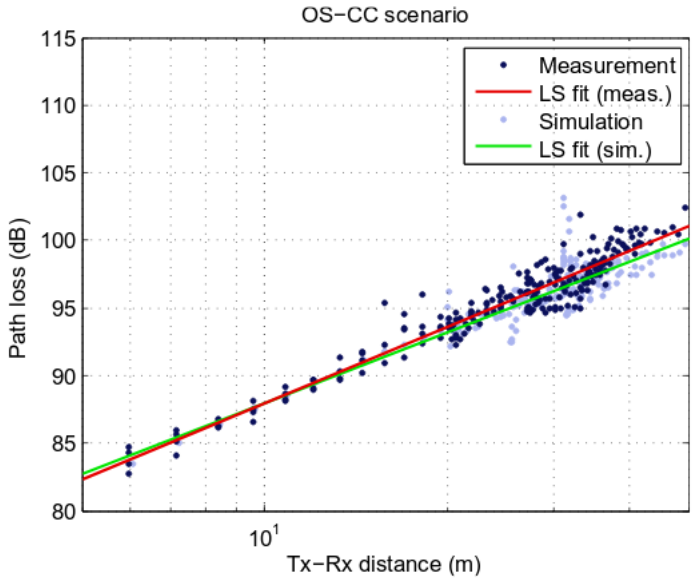

Figure 4.9 – The path loss measured results as a function of the distance between the transmitter and receiver, presented in the paper [12].

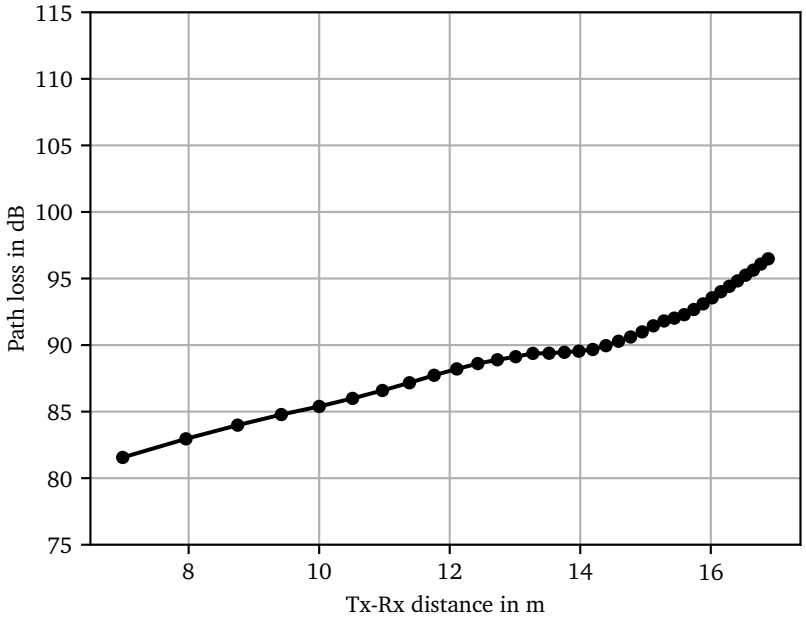

Figure 4.10 – The path loss simulation results as a function of the distance between the transmitter and receiver.

Power Delay Profile – The second metric that is analyzed is the APDP. The scenario considers the receiver moving along a linear track in a distance from the transmitter starting from 25 to 50 m. The averaging is done over a receiver movement of 10 cm corresponding to 250 data points as described in the paper [12]. After running the simulations the resulting plot is given in Figure 4.12. It is important to emphasize that the results presented in Figure 4.12 are obtained from only one simulation run.

At the start of the simulations, the distance between the transmitter and the receiver is 25 m, and as a result, the first MPC reaches the destination with a delay approximately of 83 ns. As the distance increases due to the receiver mobility, the time when the first MPC reaches the destination increases as well. For the distance of 50 m the first component from the LOS path reaches the receiver after approximately 167 ns. But as the propagation delay increases, the received power will decrease due to the longer distance. As a result of the decrease in the received power, the number of the MPC reaching the receiver with a power higher than the threshold −130 dBm, will decrease. Consequently, the number of clusters will decrease as well.

In terms of the received power, the simulation results presented in Figure 4.12, are characterized by higher values compared to the measurement results depicted in Figure 4.11. The difference in the received power reaches values in the range of 20 dB, however the behavior of the results over time is similar. The reason for the

difference between the simulation results and measurement results can be the fact that the channel model is stochastic. In the case of the number of clusters and the propagation delay, the comparison becomes more difficult. Due to the low visibility, the number of the clusters and the corresponding propagation delays for each MPC can not be exactly distinguished from the plot in Figure 4.11.

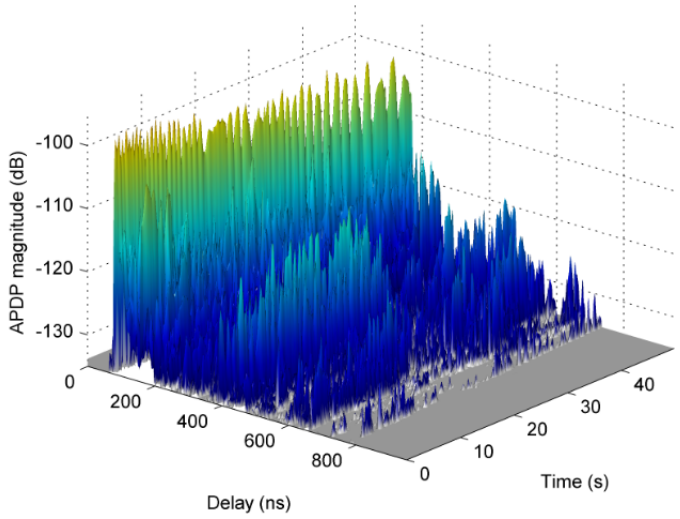

Figure 4.11 – The measured APDP for the scenario when the receiver moves in a distance from 25 to 50 m, presented in the paper [12].

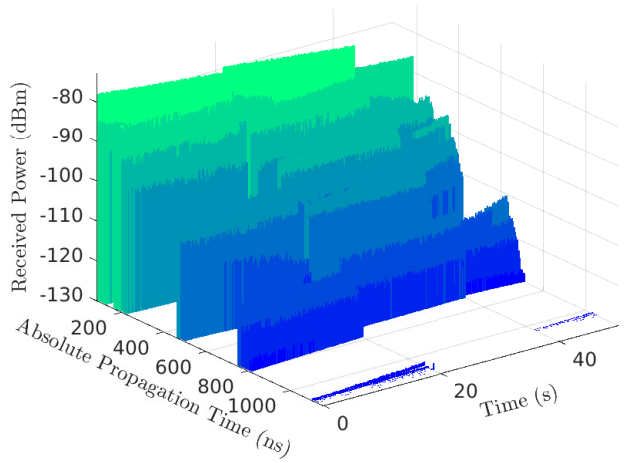

Figure 4.12 – The APDP obtained from the simulations, for the scenario when the receiver moves in a distance from 25 to 50 m.

It is important to emphasize that the mean excess delay is a crucial parameter influencing the results. This parameter is estimated following the same procedure

described in the previous validation scenarios, but for this specific scenario is very difficult to approximate it from the measurement results due to the low visibility.

In conclusion, the simulator drop based model and spatial consistency model, are validated using the outdoor measurement results at 60 GHz, presented in several papers. The simulation results are compared over the measurement results in terms of different metrics. Overall the behavior of the plots from the simulation results is similar to the corresponding measurement results, with some deviation in the values. The reason for this deviation can be the fact that some parameters for the simulations are approximated from the presented measurement results, due to the absence of this information in the corresponding papers. Besides, the channel model simulator is a stochastic channel model, which can be another factor contributing to this deviation. As a result, the channel model simulator is adequate to use for analyzing the impact of rain and snow in radio links at 60 GHz.

Chapter 5

Methodology

This chapter describes the fading prediction methods that are used for estimating the attenuation from rain and wet snow. A brief description of the implementation of these models is provided, along with the integration with the simulator. In the end, the results obtained from the validation of implemented methods are presented.

5.1 Fading Prediction Methods

The following two subsections, describe the fading prediction methods for estimating the attenuation from rain and wet snow.

5.1.1 Rain Fading Prediction Method

The fading prediction method that I have selected to use for estimating the attenuation from rain is an empirical step by step approach described in ITU-R P. 530-17 [20] using the regression coefficients specified in ITU-R P. 838-3 [28].

The first step for computing the attenuation from rain is to calculate the *specific rain attenuation* γ_R(dB/km) for a given rain rate R(mm/h) using the following power-law relationship:

$$\gamma_R = kR^{\alpha} \tag{5.1}$$

The regression coefficients k and α are a function of the frequency (from 1 to 1000 GHz) and polarization and can be derived using the formulas given in ITU-R P. 838-3 [28]. The ITU-R P. 838-3 standard itself provides the values of the regression coefficients for the horizontal and vertical polarization in a specific range of frequencies, including 60 GHz. The variation in terms of polarization is a consequence of the raindrop shapes. As described in Section 3.2, the shape of the raindrop resembles a sphere for diameters smaller than 2 mm, and as the diameter increases, the shape becomes more flattened in the bottom and wider on the sides. As a consequence of

the shape, the attenuation for the horizontal polarization is larger compared to the vertical polarization.

However, the main component for determining the specific rain attenuation is the rain intensity R given in mm/h. The model itself makes use of the value of the rain intensity with an integration time of 1 min and exceeded for the 0.01 % of an average year [15]. The integration time concept is related to the sampling time of the rain gauge used for measuring the rainfall amount. The value of the rainfall intensity exceeded for the 0.01 % of an average year can either be obtained from local long term measurements or in case this information is not available the ITU has published some digital maps in ITU-R P. 837-7 [29] along with a method described in Annex 1 of ITU-R P. 837-7 [29] and a software[4] for obtaining the value of the rain intensity exceeded for the 0.01 % of an average year with an integration time of 1 min for a specific location. The digital maps provided by ITU have been developed using the databases of the Global Precipitation Climatology Centre and the European Centre of Medium-Range Weather Forecast. In my work, I am interested to explore the value of attenuation for different scenarios and different values of the rain rate, for this reason, I am not restricted to a particular location. For simplicity, in my calculations, I am assuming that the integration time is 1 min and the percentage probability of exceedance is 0.01 %.

Furthermore, the specific rain attenuation for a given rainfall intensity depends on the type of the Rain Drop Size Distribution (DSD) used, which gives the distribution density of the raindrop diameters. As mentioned in [30], for a given rain rate, the DSD is a function of the climate zone. For temperate climate, the most widely used DSD is the Laws and Parson distribution [30], which at the same time has been used in the ITU-R model [31]. On the contrary, the tropical and equatorial regions are characterized by higher rainfall intensities and as a consequence by different DSD. As mentioned in various papers, the ITU-R model does not perform well in these regions [4].

Secondly, to get the total attenuation from rain (dB), the specific rain attenuation (dB/km) is multiplied with the effective distance d_{eff}, mathematically provided in Equation 5.2:

$$A = \gamma_R d_{eff} = \gamma_R dr \tag{5.2}$$

The effective distance is given as a multiplication of actual path length between the transmitter and receiver and the distance factor r, given in Equation 5.3:

$$r = \frac{1}{0.477 d^{0.633} R_{0.01}^{0.073\alpha} f^{0.123} - 10.579(1 - \exp(-0.024 d))} \tag{5.3}$$

[4] https://www.itu.int/en/ITU-R/study-groups/rsg3/Pages/iono-tropo-spheric.aspx?View=%7B36b3168f-af49-4c95-9854-34a89b02bb35%7D&SortField=Title&SortDir=Asc

According to ITU-R P. 530-17 [20], the maximum recommended value for the distance factor is 2.5, in this way, for the values of the denominator smaller than 0.4, the value of r is 2.5. The purpose of the multiplication between the propagation distance and the distance factor is to capture the inhomogeneity, or the variation of the rain rate in the propagation path [15].

5.1.2 Snow Fading Prediction Method

For estimating the attenuation from wet snow I have implemented the combined method for rain and wet snow described in ITU-R P. 530-15 [18]. It is important to emphasize that the combined method for rain and wet snow is changed over the years. The method described in ITU-R P. 530-17 [20] is different from the one described in ITU-R P. 530-15 [18]. The reason why I did not select the method described in ITU-R P. 530-17 [20] is that this method is based on many other standards developed by the ITU-R, making it very hard to explore the attenuation values for different scenarios.

The method described in ITU-R P. 530-15 requires two important inputs: first, the estimated rain attenuation for a specific rain intensity computed using the rain fading prediction method described in Section 5.1.1, and secondly the mean rain height, h_{rainm}. In the cases when the mean rain height, h_{rainm}, is not known for a specific location, it can be calculated using the formula given in ITU-R P. 839 [32] which computes the value of the mean rain height from the mean annual 0° isotherm height above the mean sea level. The 0° isotherm height represents the altitude at which the temperature is 0° and varies with the geographical position. One way to obtain it for a specific location is by using the digital map provided in ITU-R P. 839 [32].

Once the two input values have been computed, the following steps are used to determine the multiplying factor used for estimating the attenuation from combined rain and wet snow.

Step 1. Calculate the rain height at the center of the path link, using as an input the height above the mean sea level of the transmitter and receiver antennas as given in Equation 5.4:

$$h_{link} = 0.5(h_1 + h_2) - (D^2/17) \tag{5.4}$$

where

- $h_{1,2}$ are the height of the link terminals above the mean sea level
- D is the path length in km

Step 2. Once the rain height at the center of the communication link has been calculated, a test must be made to investigate whether the path is or not affected by

the wet snow or the melting layer. The effect of the melting layer might be present for high latitudes or in cases of high link altitudes.

$$h_{link} \leq h_{rainm} - 3600 \tag{5.5}$$

In the cases when the test is not passed then, the communication link is not affected by the melting layer, otherwise, the following steps should be taken to estimate the corresponding attenuation value.

Step 3. The rain height variability is modeled by taking 49 intervals of 100 m relative to the h_{rainm}. The multiplying factor is computed for each interval (represented by index i) from the Equation 5.6.

$$\Delta F = \Gamma(\Delta h) P_i \tag{5.6}$$

where:

- Δh is the link height relative to the rain height calculated for each interval using Equation 5.7

  $$\Delta h = h_{\text{link}} - h_{\text{rain}} \tag{5.7}$$

  where:

  - h_{rain} is the rain height computed using Equation 5.8:

    $$h_{rain} = h_{rainm} - 2400 + 100i \tag{5.8}$$

- P is the probability that the calculated rain height will be in the corresponding interval. The values of this parameter can be obtained from Table 1 in ITU-R P. 530-15 [18].

- $\Gamma(\Delta h)$ is a multiplying factor considering the specific attenuation for the corresponding link height relative to the rain height computed from Equation 5.9:

$$\Gamma(\Delta h) = \begin{cases} 0 & 0 < \Delta h \\ \dfrac{4\left(1-e^{\Delta h/70}\right)^2}{\left(1+\left(1-e^{-(\Delta h/600)^2}\right)^2\left(4(1-e^{\Delta h/70})^2-1\right)\right)} & -1200 \leq \Delta h \leq 0 \\ 1 & \Delta h < -1200 \end{cases} \tag{5.9}$$

Step 4. The computed values of the multiplying factor for each interval are added up, giving the total multiplying factor.

$$F = F + \Delta F \tag{5.10}$$

Step 5. The attenuation from combined rain and wet snow is computed using the following formula.

$$A_{rs} = A_p F \tag{5.11}$$

where:

- A_p is the estimated rain attenuation

5.2 Implementation Details

The NYUSIM is implemented in MATLAB, which is a computing environment and a programing language based on matrix, developed by MathWorks.

Since the goal of my thesis is to study the impact of rain and wet snow on the signal propagation at 60 GHz, I have to integrate the implementation of the corresponding fading prediction methods on top of the NYUSIM. For this reason, I have implemented the fading prediction methods described in Section 5.1.1 and Section 5.1.2 also in MATLAB.

For the rain fading prediction method, MATLAB offers the function *rainpl*[5], which computes the attenuation from rain as a function of the rain intensity, frequency, communication distance, elevation angle, and tilt angle of polarization. This function computes the attenuation from rain based on the fading prediction method described in [19], which is an old version of the fading prediction method provided by the ITU and has been changed over the years. As a result, I have decided not to use the function provided by MATLAB, but to do the implementation following the steps described in Section 5.1.1.

After implementing the fading prediction methods, the next step is to integrate these methods into the channel model simulator for both the drop based model and the spatial consistency model. The channel model simulator used in this thesis is the NYUSIM Version 2.0. Both the fading prediction methods compute the attenuation from rain and combined rain and wet snow in decibel. Depending on the scenario (if there is only rain present or combined rain and wet snow), the attenuation estimated from the corresponding prediction method is added to the total path loss calculated using the Equation 4.1.

Equation 4.1, for computing the path loss, is comprised of a term that gives the atmospheric attenuation from dry air (including O_2), water vapor (H_2O), rain and haze, as described in Section 4.1.1. Since from the rain fading prediction method I am estimating the attenuation from rain, I have removed the simulator implementation for calculating the rain attenuation.

[5] `https://uk.mathworks.com/help/phased/ref/rainpl.html`

5.3 Validation of the fading prediction methods

This section describes the results that are obtained from the validation of the fading prediction methods.

5.3.1 Validation of Rain Attenuation Prediction Method

Once the rain fading prediction method is implemented, the validation is necessary to verify the accuracy of the method. For this purpose, I have selected two papers that are using the same method for calculating the attenuation from rain. The first paper is used to compare the behavior of the specific rain attenuation under different conditions and the second paper is used to analyze the behavior of the rain attenuation, focusing on the distance factor.

Specific Rain Attenuation – The first paper is focused on analyzing the rain rate and the rain attenuation metrics at 26 GHz in Malaysia, by conducting real measurements and comparing the results with the ones predicted by the method described in ITU-R P. 530-16 using the parameter values from ITU-R P. 838-3. The prediction method has also been used to explore the dependency of the rain fading from the rain rate, operating frequency, effective path length, and polarization type.

The specific rain attenuation is computed using the implemented prediction method for the same input parameters as the ones presented in the paper to compare the results. The rain fading prediction method described in ITU-R P. 530-16 standard, used by the authors of the paper, is the same as the method presented in ITU-R P. 530-17, used for the simulations. It is important to emphasize that the following results from the paper, are not observed from the measurements, but are results obtained from the same method to study the dependency of the rain attenuation from various factors.

First, the authors in [4] have analyzed the impact of the rain intensity on the specific rain attenuation, at various operating frequencies and for two polarization types as shown in Figure 5.1 and Figure 5.2. The values of the rain intensity vary from 10 to 270 mm/h. The results indicate that at a fixed frequency as the intensity of the rainfall increases, the specific attenuation increases rapidly. This is because as the rain intensity increases, the density of the raindrops on the distance unit increases at the same time. As a result, the probability that the electromagnetic wave will hit a raindrop during the propagation will increase, leading to higher absorption and scattering. For instance, at 60 GHz, the attenuation reaches values in the range of 56 and 62 dB/km for the rainfall intensity of 270 mm/h for the horizontal and vertical polarization respectively. This large value of the attenuation shows clearly the strong impact of rain on signal propagation, especially at heavy rainfall, as 270 mm/h. Besides the rain rate, polarization is another factor influencing the signal

propagation. The results in Figure 5.1 for the horizontal polarization depict higher values of the specific rain attenuation compared to the results in Figure 5.2 for the vertical polarization. The difference between the polarizations is larger during heavy rainfall when the raindrops are larger and as a consequence non-spherical.

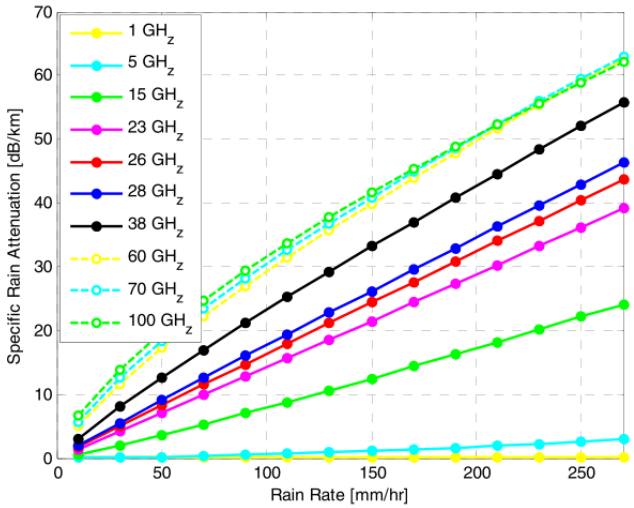

Figure 5.1 – The impact of the rain rate on the specific rain attenuation for different frequencies and horizontal polarization, presented in the paper © 2018, IEEE [4].

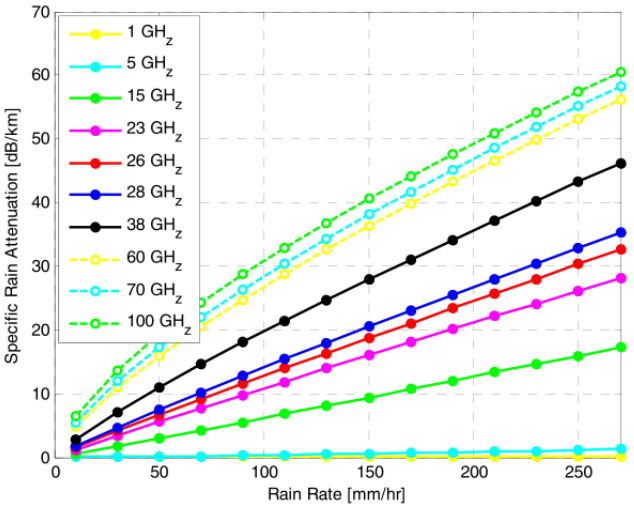

Figure 5.2 – The impact of the rain rate on the specific rain attenuation for different frequencies and vertical polarization, presented in the paper © 2018, IEEE [4].

At the same time, the implemented method is used to compute the values of the specific rain attenuation, for the same range of rain intensities, at frequencies 23, 38, 60, and 70 GHz. The results obtained from the simulations are shown in Figure 5.3 for the horizontal polarization and in Figure 5.4 for the vertical polarization. The values of the regression coefficients, for the corresponding frequencies, used for the calculations are given in Table C.1 of Appendix C. The computed specific rain attenuation values at the aforementioned frequencies are quite similar to the corresponding published results, for different values of the rain rate. This similarity can be observed at the ranging values of the specific rain attenuation at different frequencies, for example at 60 GHz, for the values of the rain rate from 10 to 270 mm/h, the value of the specific rain attenuation ranges approximately from 5 to 62 dB/km for horizontal polarization and from 4.8 to 56 dB/km for the vertical polarization.

The specific rain attenuation is also studied as a function of the frequency for different rain intensities and polarization types. The results published in the paper are shown in Figure 5.5 for the horizontal polarization, and in Figure 5.6 for the vertical polarization.

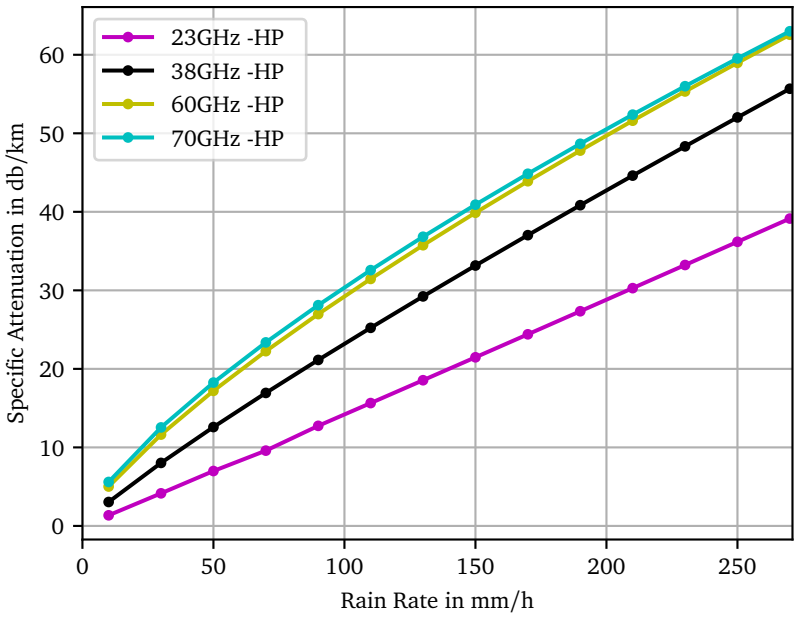

Figure 5.3 – The impact of the rain rate on the specific rain attenuation for different frequency and horizontal polarization, from the simulations.

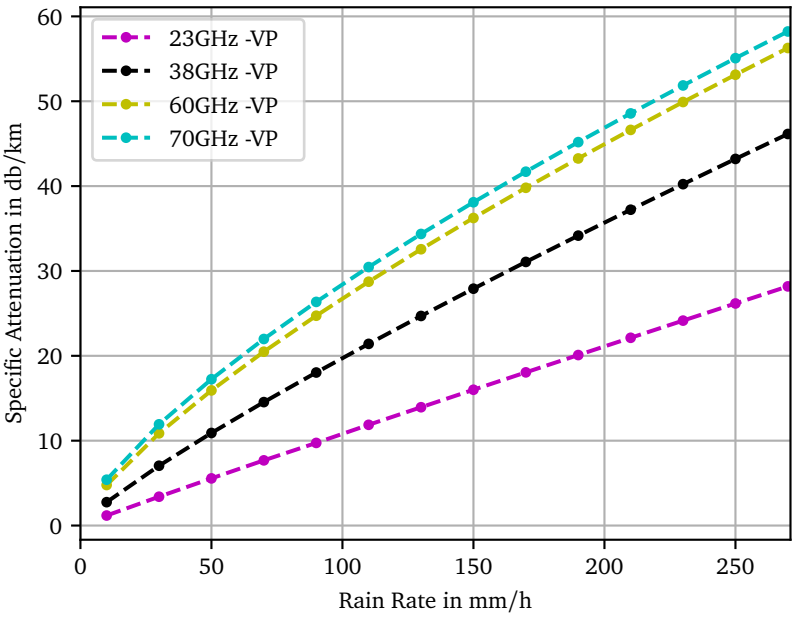

Figure 5.4 – The impact of the rain rate on the specific rain attenuation for different frequency and vertical polarization, from the simulations.

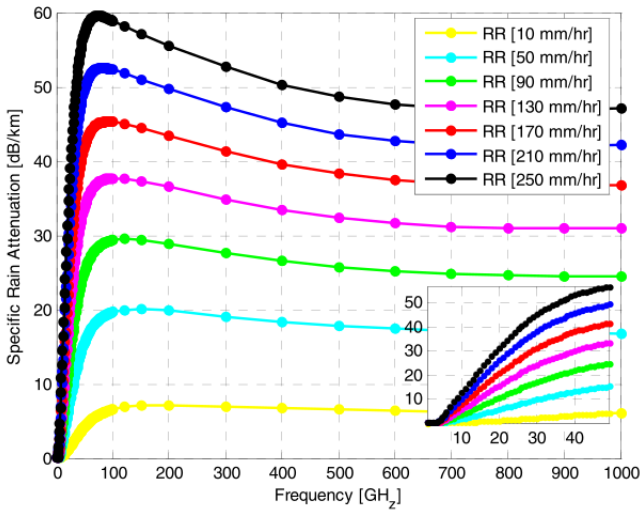

Figure 5.5 – The impact of the frequency on the specific rain attenuation for different rain rates and horizontal polarization, presented in the paper © 2018, IEEE [4].

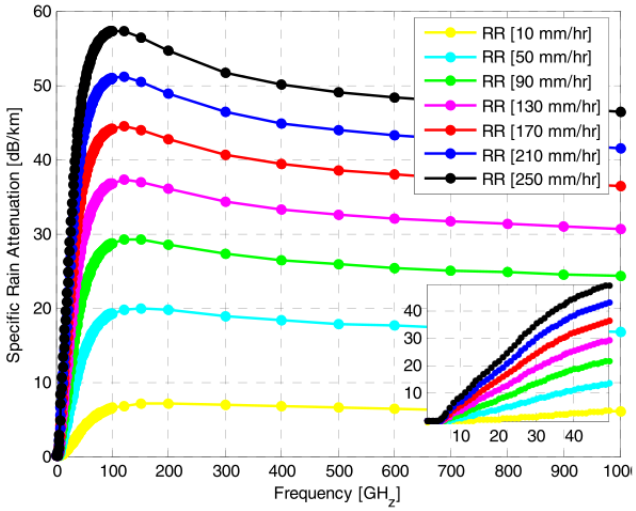

Figure 5.6 – The impact of the frequency on the specific rain attenuation for different rain rates and vertical polarization, presented in the paper © 2018, IEEE [4].

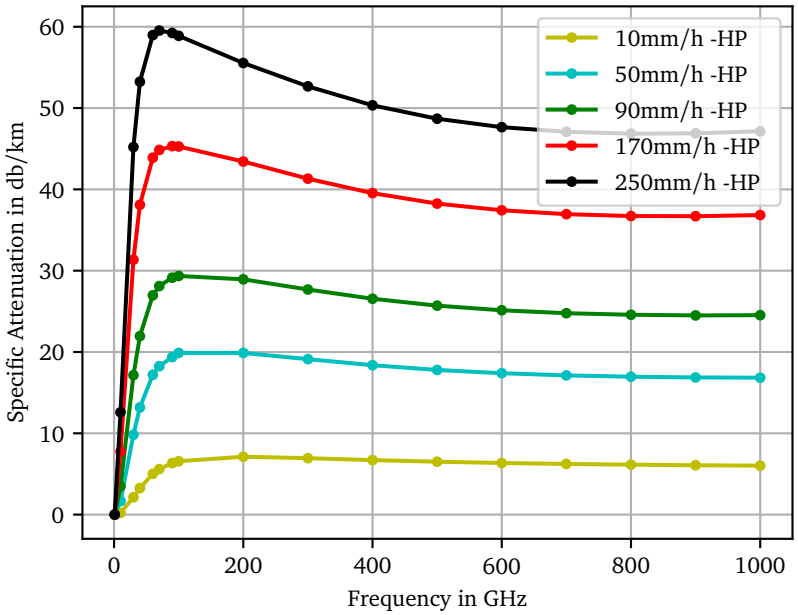

Figure 5.7 – The impact of the frequency on the specific rain attenuation for different rain rate and horizontal polarization, from the simulations.

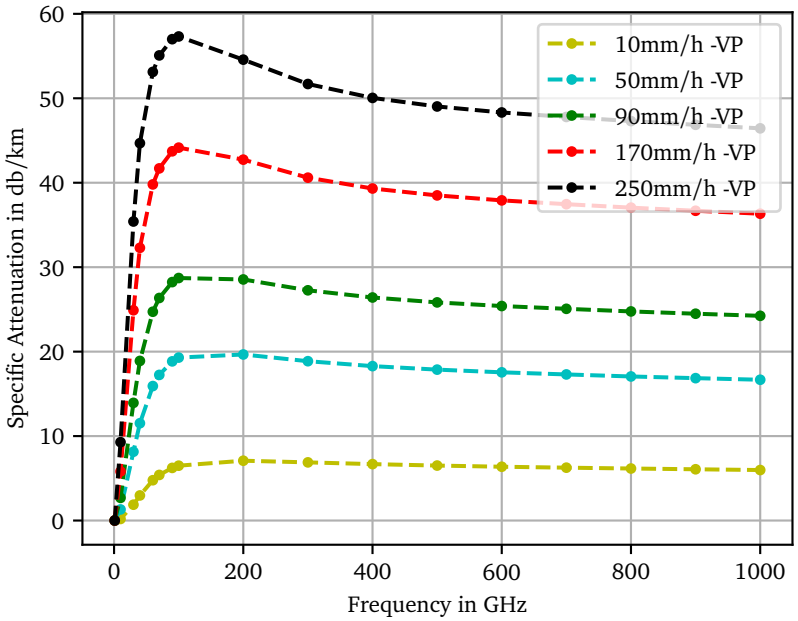

Figure 5.8 – The impact of the frequency on the specific rain attenuation for different rain rate and vertical polarization, from the simulations.

As mentioned in the paper [4] as the operating frequency increases, the specific rain attenuation increases proportionally. This comes as a result of the electromagnetic wavelength, which decreases in the order of the raindrop size at high frequencies. As a consequence, the interchange of energy because of the absorption and scattering also increases once the electromagnetic wave hits the raindrop. As mentioned in [33] the rain attenuation for frequencies higher than 90 GHz is almost constant, and this is also visible from the plot of the specific rain attenuation as a function of the frequency. Furthermore, the difference in values due to the polarization is more visible for frequencies below 100 GHz, and it gets smaller for higher frequencies. According to [21] the difference in the attenuation coefficients gets smaller for frequencies above 100 GHz, as a result of the very short wavelength, which increases the weight of the attenuation due to small raindrops that can be considered spherical. The values of the specific rain attenuation have been also computed using the implemented model for the range of frequencies from 1 to 1000 GHz and the values of the rain rate 10, 50, 90, 170 and 250 mm/h. The values of the regression coefficients, for each frequency and polarization, used for the simulations, are given in Table C.1 of the Appendix C. The results from the simulations are given in Figure 5.7 for the horizontal polarization and in Figure 5.8 for the vertical

polarization. These results, for the corresponding rain intensities and polarization are similar to the results published in the paper [4].

Rain attenuation – The purpose of the paper [15] is to compare the performance of different fading prediction methods that are available for terrestrial links, and to use the most relevant one to do the transformation of rain attenuation on links having different parameters (frequency, polarization, and distance). Since the communication links in mmWave are limited to short distances, while most of the existing measurement data are collected over long communication distances, the paper proposes a transformation method which extracts the rain intensity from the rain attenuation and uses this value as an input to calculate the attenuation on links with hypothetical parameters focusing on short distance. The method proposed in ITU-R P. 530-15 is one of the investigated methods from the paper, which at the same time gives the best performance in the link transformation [15]. The scenario that I have selected for the validation is the one depicted in Figure 5.9, which shows the value of the rain rate estimated from the total measured rain attenuation.

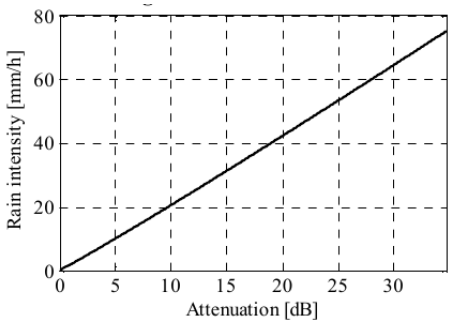

Figure 5.9 – The relation between the rain intensity and the corresponding attenuation as given in the paper © 2016, IEEE [15]. The values of the rain intensities are estimated from the measured rain attenuation.

The values of the rain attenuation, regression coefficients and the distance factor are from the measured real link. The implemented method has been validated using the input parameters given in Table 5.1. It is important to emphasize that the fading prediction method described in ITU-R P. 530-15, used by the paper, is the same as the fading prediction method presented in ITU-R P. 530-17, used in the implementation.

The rain intensity takes values in the range from 10 to 70 mm/h, as given in Figure 5.9. The value of the operating frequency, polarization and the distance between the transmitter and receiver are taken from the paper, while the values of the regression coefficients are determined from ITU-R P. 838-3 for the corresponding frequency. The results collected from the simulations are presented in Figure 5.10.

Table 5.1 – Summary of the simulation parameters used for calculating the attenuation from rain for different rain intensities.

Parameter	Values
Rain Rate	0, 10, 20 .. 70 mm/h
Frequency	38 GHz
Distance	1.5 km
Polarization	Horizontal (HP)
k (HP)	0.4001
α (HP)	0.8816

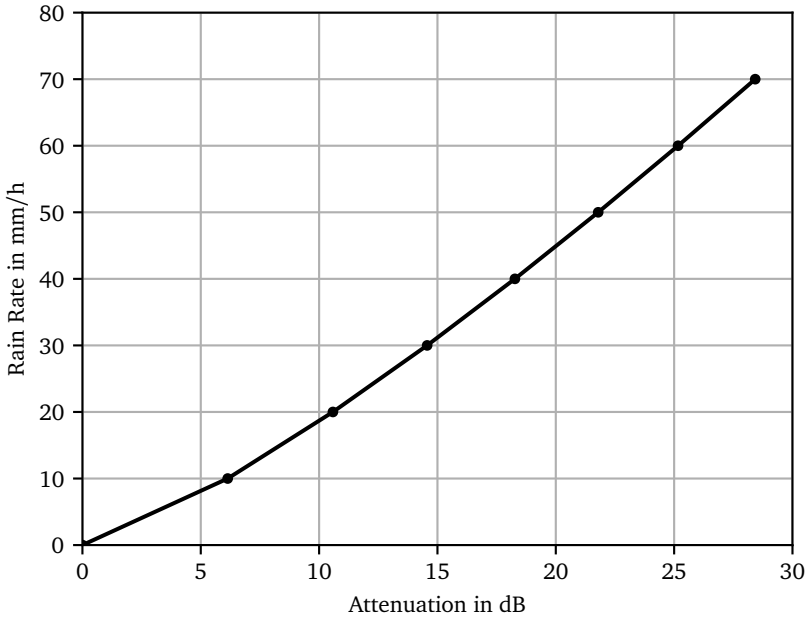

Figure 5.10 – The relation between the rain intensity and the corresponding attenuation using the implemented method.

The simulation results follow similar behavior as the results published in the paper. The value of the attenuation increases linearly as the intensity of the rain rate increases. Different from the case of the paper where the value of the rain rate is estimated from the total rain attenuation, in my simulations, the value of the rain rate is an input to the equation for calculating the total rain attenuation. Although the curve follows the same behavior as the one given in Figure 5.9, the attenuation values for each rain intensity experience a deviation in the range -4 to +2 dB. This deviation gets larger as the value of the intensity of the rain increases.

5.3.2 Validation of Snow Attenuation Prediction Method

For the validation of the prediction method that estimates the attenuation from combined rain and wet snow, I have selected two papers where the value of attenuation has been computed only for one specific scenario. Differently from the case of rain, the number of papers available for validating the prediction method for combined rain and wet snow is very limited.

First Validation Scenario – The purpose of the first paper [16] is to explore the attenuation from precipitations, mainly rain and wet snow. It presents the attenuation values from measurements conducted over 3 years on a 11.1 km long radio link at 26 GHz and compares the values with the ones estimated using the fading prediction method presented in ITU-R P. 530-15 [18]. The method uses as input the estimated rain attenuation value computed from the rain fading prediction method, described in Section 5.1.2. For this reason first, the specific rain attenuation and the total rain attenuation are computed for the horizontal and vertical polarization using the regression coefficients provided by ITU-R P. 838-3. Then, given the values of the transmission and receiver antennas heights and the mean rain height, for the specific location, the value of the multiplying factor is computed. It is important to emphasize that the values are calculated using the fading prediction methods and are not collected from the measurements.

The same parameters are used as input in the implemented prediction method for estimating the multiplying factor. A list of the input parameters is given in Table 5.2. The estimated specific rain attenuation, rain attenuation and the multiplying

Table 5.2 – A list of parameter values for estimating the attenuation from the combined rain and wet snow using the fading prediction method.

Parameter	Values
Rain Intensity	34 mm/h
Frequency	26 GHz
Distance	11.1 km
h_1	600 mamsl
h_2	60 mamsl
h_{rainm}	1815 km
k_H	0.1724
k_V	0.1669
α_H	0.9884
α_V	0.9421

factor obtained from the implemented methods are exactly the same as the ones presented in the paper and are given in Table 5.3.

The specific rain attenuation and the total rain attenuation have larger values for the horizontal polarization due to the shape of the drop, which is wider on the sides and flattened in the bottom. As a result, the attenuation from combined rain and wet

Table 5.3 – The estimated results from the implemented prediction method.

Parameter	Values
$\gamma_r HP$	5.63 dB/km
$\gamma_r VP$	4.63 dB/km
Rain attenuation HP	35.88 dB
Rain attenuation VP	30.38 dB
Multiplying factor	1.18

snow will be as well larger for the case of the horizontal polarization, since the rain attenuation is used as an input in the fading prediction method. The attenuation from the combined rain and wet snow is given as a multiplication of the attenuation from rain for a given polarization and the multiplying factor as given in Equation 5.11. Since the value of the multiplying factor is 1.18, the attenuation from the combined rain and wet snow is larger compared to the case when there is only pure rain present in the transmission medium. The reason behind this result is the fact that the particles in the melting layer (wet snow) are larger than the normal raindrops and attenuate the same as the drop was entirely water, as explained in Section 3.3.

Second Validation Scenario – The purpose of the second paper [17] is to study the impact of the combined rain and wet snow on the radio link, over an area that is characterized by the presence of wet snow during the winter season. The results obtained from the measurements conducted over a period of 18 months are compared to the results predicted by the fading prediction method described in ITU-R P. 530-15 [18]. The results estimated in the paper from the prediction method [17] are used for the validation of the implemented method. Similar to the previous scenario, the calculations are done only for a specific case. The parameter values used as input in the implemented prediction method are given in Table 5.4.

Table 5.4 – A list of parameter values for estimating the attenuation from the combined rain and wet snow using the fading prediction method.

Parameter	Values
Rain Intensity	23 mm/h
Frequency	13 GHz
Distance	43 km
h_1	475 mamsl
h_2	95 mamsl
h_{rainm}	1360 km
k_V	0.03266
α_V	1.0901

The values of the specific rain attenuation, total rain attenuation, and the multiplying factor are computed for the vertical polarization. The results are the same as the results presented in the paper and are given in Table 5.5.

Table 5.5 – The estimated results from the implemented prediction methods.

Parameter	Values
γ_r	1.0 dB/km
Rain Attenuation	18.93 dB
Multiplying factor	1.26

The results depict that the attenuation from the combined rain and wet snow will be larger than the attenuation only from rain. This is a result of the particles belonging to the melting layer which are larger compared to the normal raindrops and attenuate the same as the particles were entirely water.

Chapter 6

Evaluation

This Chapter analysis the impact of rain and wet snow on signal propagation at 60 GHz, through the simulation results. First, Section 6.1 presents the configuration setup used for running the simulations, then Section 6.2 describes the collected results.

6.1 Simulation Setup

Mmwave communications can be used in various applications. To analyze the effect of the atmospheric variations in these links requires first to determine the communication scenario. The scenario that I have selected is the car to car communication, considering always the presence of a LOS component, with short communication distance ranging from 1 to the maximum 200 m as shown in Figure 6.1.

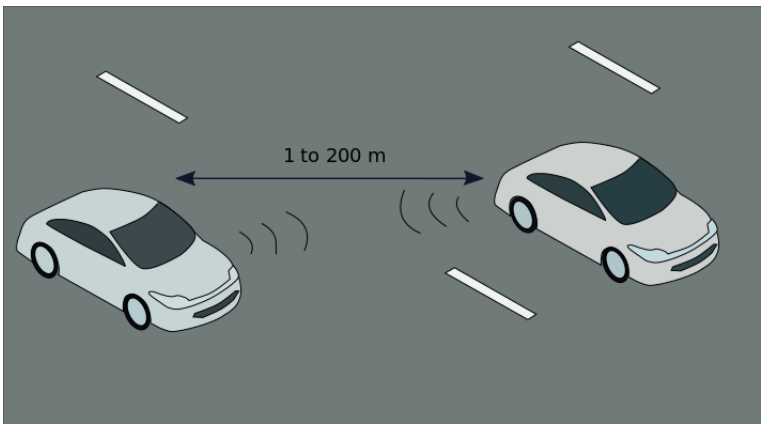

Figure 6.1 – The simulation scenario.

After fixing the scenario, the next important step, in order to study the effect of rain and wet snow is to define the corresponding intensities for running simulations. In Section 3.2, it is mentioned that a possible classification of rain is based on the intensity. This classification divides the rain into light, moderate and heavy [34] using threshold values set according to the local climate. In order to choose these values according to the local climate, I used the classification provided by the German Meteorological Service[6], as given in Table 6.1.

Table 6.1 – Rain classification based on the intensity, according to the German Meteorological Service.

Classification	Threshold
Light	< 2.5 mm/h
Moderate	2.5–10 mm/h
Strong	≥ 10 mm/h
Very Strong	≥ 50 mm/h

This classification divides the rain based on the intensity into light, moderate, strong and very strong. The same information source is used to obtain the classification for the wet snow (combined rain and snow) as given in Table 6.2.

Table 6.2 – Combined rain and snow classification based on the intensity, according to the German Meteorological Service.

Classification	Threshold
Light	< 1 mm/h
Moderate	1–5 mm/h
Strong	≥ 5 mm/h

Since the fading prediction method for combined rain and wet snow uses the rain attenuation as input, the values taken from the German Meteorological Service for the classification of the wet snow are used as input rain intensities.

The selected intensities values for the simulations are given in Table 6.3 for rain and in Table 6.4 for the wet snow.

Table 6.3 – The selected rain intensity values for computing the attenuation from rain.

Classification	Values
Light	2 mm/h
Moderate	10 mm/h
Strong	50 mm/h
Very Strong	100 mm/h, 150 mm/h, 250 mm/h

[6] https://www.dwd.de/DE/service/lexikon/Functions/glossar.html?lv2=101812&lv3=101906

Table 6.4 – The selected rain intensity values for computing the attenuation from wet snow.

Classification	Values
Light	1 mm/h
Moderate	5 mm/h
Strong	10 mm/h

In the case of rain, an extra limit value of 250 mm/h is taken into consideration, which according to [4], is a very strong rain intensity, characterizing the tropical and equatorial climates. Even though this value is not a characteristic of the local temperate climate, I have considered it in my calculations as a good reference to compute a maximum possible attenuation.

In order to estimate the attenuation from rain and wet snow using the fading prediction methods, I have to decide about a few important parameters related to these methods. First, to compute the specific rain attenuation, described in Section 5.1.1, the values of the regression coefficients are determined for the horizontal and vertical polarizations. Since my work is focused on the communication frequency 60 GHz, the values of the regression coefficients are fixed and are given in Table 6.5. These values are provided by the ITU-R P. 838-3 [28]. Secondly, similarly to the rain

Table 6.5 – The regression coefficient values for the rain fading prediction method.

Parameters	Values
k_H	0.8606
k_V	0.8515
α_H	0.7656
α_V	0.7486

method, I have to define a few parameter values related to the prediction method for combined rain and wet snow described in Section 5.1.2. The values of these parameters are given in Table 6.6. The first two parameters are the corresponding

Table 6.6 – The parameter values for the prediction method for combined rain and wet snow.

Parameters	Values
h_1	1.5 m
h_2	1.5 m
h_0	2000 m
Altitude	122 m

transmitter and receiver antenna heights, h_1 and h_2, which are defined as 1.5 m, considering that the scenario is the car to car communication. The mean annual 0 °C isotherm height above the mean sea level is the input for computing the mean

rain height. Since the 0 °C isotherm height varies with the geographical position, the location that I select for my simulations is Paderborn city. For obtaining the aforementioned parameter I use the digital map provided in ITU-R P. 839 [32] and the approximate value is 2000 m. The last parameter is the altitude, which for Paderborn is approximated as 122 m[7].

Furthermore, there are a few other parameter values that have to be fixed, related to the channel model simulator in order to run simulations. The most relevant parameters for both the drop based model and the spatial consistency model are listed in Table 6.7 and Table 6.8.

Table 6.7 – The list of the parameter values selected for the simulations.

Parameters	Values
Frequency	60 GHz
RFBW	250 MHz
Environment	LOS
Tx Power	15 dBm
Antenna Gain	2 dBi
PLE	2
SF	4
Number of Clusters	6
Number of Subpaths	15

Table 6.8 – Some extra parameters for the spatial consistency model.

Parameters	Values
Update Distance	1 m
Correlation Distance	10 m
Velocity	0.5 m/s

After defining the scenario and the parameter values, I run simulations to collect data for different metrics, in order to analyze the influence of the weather variations on the mmWave communication links. The metrics are divided into two groups: the ones related to the fading prediction methods and the ones related to the channel model simulator.

The following metrics are from the fading prediction methods:

Specific Rain Attenuation – is the rain attenuation in decibel per unit distance as a function of the rain rate, frequency, and polarization. Since the frequency in this case is fixed to 60 GHz, this metric is a good indicator of the dependency of the attenuation from the rain intensity and polarization.

Rain Attenuation – gives the attenuation from the rain in decibel using as an input the specific rain attenuation and the effective distance. To capture the rain

[7] `https://www.mapcoordinates.net/en`

inhomogeneity through the transmission medium, the communication distance is multiplied by the distance factor giving the effective distance as described in Section 5.1.1. This metric is a good indicator of the rain attenuation dependency from the communication distance.

Wet Snow Attenuation – gives the attenuation in decibel from the presence of the combined rain and wet snow in the transmission medium. The computation requires as input the rain attenuation as described in Section 5.1.2.

The following metrics are from the channel model simulator:

Path Loss – represents the total signal attenuation and is given in decibel. The NYUSIM uses the CI free space reference distance path loss model described in Section 4.1.1, for computing the total path loss. The component in the described model for capturing the atmospheric attenuation (from the water and oxygen molecules, etc), is not considered in the simulations. This component is a function of the temperature, humidity, and atmospheric pressure, which take different values depending on the weather conditions. Considering that in 60 GHz, the attenuation from the oxygen molecules reaches the peak value, an exact calculation of this term might be important. Due to the lack of information regarding the temperature, humidity, and atmospheric pressure I have decided to remove this term from the simulations and study it divided.

Power Delay Profile – gives the received power for each MPC as a function of the corresponding propagation delay. The number of the time clusters and the subpath components are fixed, for the drop based model, in order to conduct multiple simulations and average the results. The number of time clusters is fixed as 6, and the number of subpath components as 15. To compare the results with the spatial consistency model, the same fixed numbers of time clusters and subpath components are used for the spatial consistency model.

6.2 Results

The following subsections describe the observations from the simulations. First, it starts with the metrics associated with the fading prediction methods, followed by the metrics associated with the simulator.

6.2.1 Specific Rain Attenuation

The specific rain attenuation in dB/km is a good indicator of the attenuation dependency from the rain intensity and polarization. After running the simulations, the results obtained for the horizontal and vertical polarization, are given in Figure 6.2. The plot indicates that the specific rain attenuation increases as the rain rate increases. Once the rainfall intensity rises, the raindrop density in the distance unit

rises as well, as a consequence the probability that an electromagnetic wave will hit a raindrop is higher. As a result, the effect of absorption and scattering increases.

The effect of the polarization type is also visible from the plot. As explained in Section 3.2, the attenuation from the horizontal polarization is expected to be larger due to the shape of the raindrop which is more flattened in the bottom and wider on the sides. The difference in the specific rain attenuation between the two polarizations becomes more clear as the rain intensity increases since the size of the raindrops will be larger. The gap is very small for light rain but it can reach an approximate value of 8 dB/km for the rain intensity of 250 mm/h.

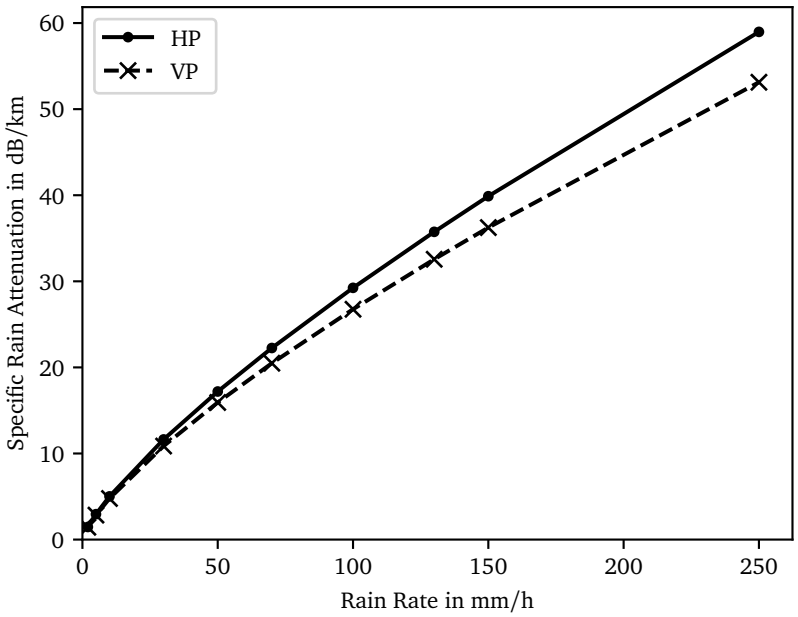

Figure 6.2 – The specific rain attenuation results as a function of rain rate, for horizontal and vertical polarization.

As shown in the plot, the specific rain attenuation can reach values in the range of 58 dB/km for rain intensities rising to 250 mm/h. Even though this large value of the rain intensity is mostly characteristic of the tropical and equatorial regions [4] and not of the temperate climate, like the one in Germany, the results depict the large effect that rain can have on the propagation signal.

6.2.2 Rain Attenuation

The rain attenuation is an important metric, that determines the total attenuation from rain, for a specific communication link. The two input parameters for computing

the rain attenuation are the specific rain attenuation and the effective distance. The effective distance is computed by multiplying the distance between the transmitter and receiver with the distance factor, for capturing the inhomogeneity of rain through the propagation link. This metric explores the influence of the distance in the total attenuation from rain.

The results obtained from the simulations are presented in Figure 6.3, which shows the attenuation from rain as a function of the communication distance for different rain intensities and polarization types (horizontal and vertical). The results for larger distances can be found in Appendix A.1. It is important to clarify that the distance depicted in the plot is the real distance between the transmitter and the receiver and not the effective distance.

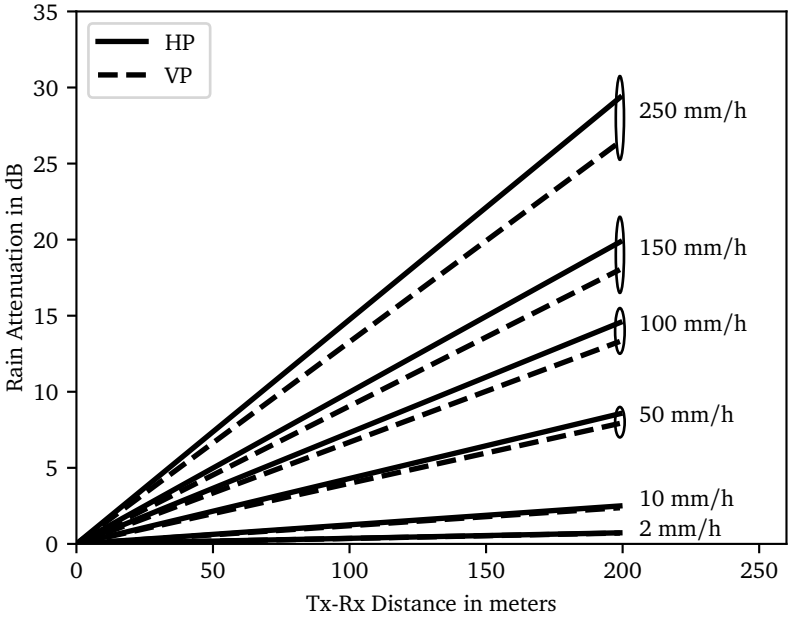

Figure 6.3 – Rain attenuation for different rain intensities and polarization types, as a function of the distance between the transmitter and receiver ranging from 1 to 200 m.

The plot depicts that there is a direct proportionality between the attenuation from rain and the communication distance. As the communication distance increases, the volume of the rain increases as well along with the effect of absorption and scattering, leading to a higher attenuation.

Secondly, the plot shows that at very short communication distance, for example, 25 m, the attenuation from rain is very small, reaching a maximum value of almost 4 dB at very strong rain intensity of 250 mm/h. As a result, the impact of the rain

is not crucial in the signal attenuation. When the distance increases, for example, 200 m, the influence of rain is yet very small in the case of light and moderate rain and it gets larger only for strong rainfalls.

Finally, the polarization type is another factor contributing to the total attenuation. As described in the case of the specific rain attenuation, the difference between the horizontal and vertical polarization is more clear for strong rainfalls and also large communication distance.

Comparison to the simulator model – The NYUSIM uses the CI free space reference distance path loss model, described in Section 4.1.1, for determining the total signal attenuation. One term of this model represents the atmospheric attenuation capturing the effect of dry air (including O_2), water vapor (H_2O), rain and haze. The calculations are based on the millimeter-wave propagation model for computing the complex refractivity for the atmospheric conditions [35]. Considering that the simulator already computes the attenuation from rain, a comparison of the results using this model and the implemented one might be interesting to observe. For computing the attenuation from rain, the simulator model requires as input the rain intensity in mm/h, the frequency, and the communication distance. The results obtained from the simulations, comparing the two models, are shown in Figure 6.4. The plot presents the values of the rain attenuation as a function of the distance between the transmitter and the receiver ranging from 1 to 200 m, for the rain intensities 10, 100 and 250 mm/h.

The first conclusion that can be observed from the plot is that the model offered by the simulator does not consider the polarization type. Considering that the shape of the raindrop has an impact on the attenuation, this might be an important component that should not be ignored.

Secondly, the estimated attenuation from the simulator model is smaller compared to the attenuation estimated using the implemented fading prediction method. Even though the results using the simulator model, follow the same behavior as the results obtained from the implemented method, these values are smaller. The difference between the results is small for the value of the rain rate of 10 mm/h even when the communication distance is 200 m. The gap increases rapidly for stronger rainfalls, especially at long communication distance.

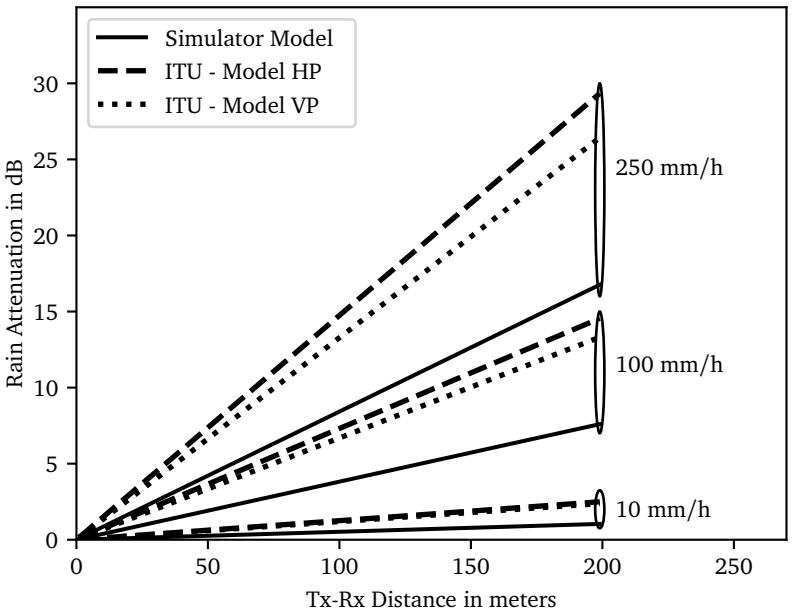

Figure 6.4 – Comparison of the rain attenuation results obtained from the ITU model for the horizontal and vertical polarization, and the model provided by the simulator.

Total atmospheric attenuation – Even though the function provided by the simulator for estimating the atmospheric attenuation, can be used without the component of rain, I have decided not to include this term in my simulations. This function requires as input three important parameters: temperature, humidity, and barometric pressure. These parameters take different values based on the weather conditions. Since at 60 GHz the attenuation from oxygen molecules reaches the peak value, an exact computation of the atmospheric attenuation, using real parameter values might be important. Considering that this information is not present for the different rain intensities, I have decided to remove this term from my calculations and study it separately. Hence I use some real weather data collected from the Paderborn University weather station[8] to compute the total atmospheric attenuation, for different scenarios. The scenarios with the corresponding parameter values are presented in Table 6.9.

For estimating the attenuation, I use the function provided by the simulator, without the component for estimating the attenuation from rain. Then I add to the computed result the rain attenuation estimated by the implemented method. The attenuation results for each scenario are given in Figure 6.5 as a function of the

[8] `http://wetter.uni-paderborn.de/`

Table 6.9 – Parameter values for three scenarios.

Parameters	Scenario 1	Scenario 2	Scenario 3
Date	November 28, 2019	November 29, 2019	November 26, 2019
Time	22:02	01:02	14:32
Bar. Press.	995.75 mbar	998.85 mbar	1004.75 mbar
Temp.	8.25 °C	7.05 °C	10.05 °C
Humidity	98 %	98.5 %	85.5 %
Rain	1 mm/h	0.4 mm/h	0 mm/h

transmission distance ranging from 1 to 200 meters. Both the rain intensities, in scenarios 1 and 2, belong to the same group of light rain classification.

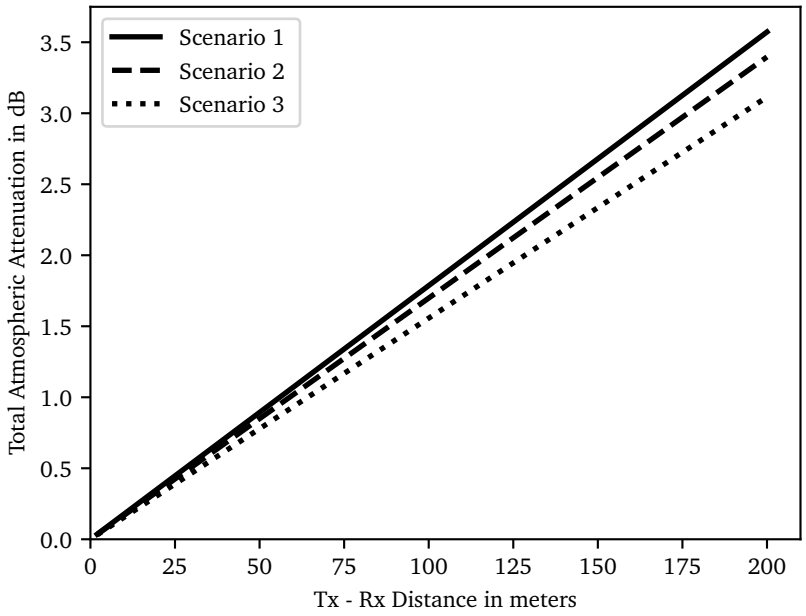

Figure 6.5 – Total atmospheric attenuation for different scenarios.

The results show that the atmospheric attenuation for the considered scenarios reaches small values. The attenuation when rain is present in the transmission medium is larger over the case when there is no rain, and it increases with rain intensity and communication distance.

6.2.3 Wet Snow Attenuation

The wet snow attenuation metric represents the total attenuation from combined rain and wet snow in the transmission medium. As explained in Section 5.1.2, the

prediction method for estimating the attenuation from combined rain and wet snow uses as an input the attenuation from rain estimated for a given rain intensity. After running the simulations for the rain intensity values given in Table 6.4, the obtained results are shown in Figure 6.6.

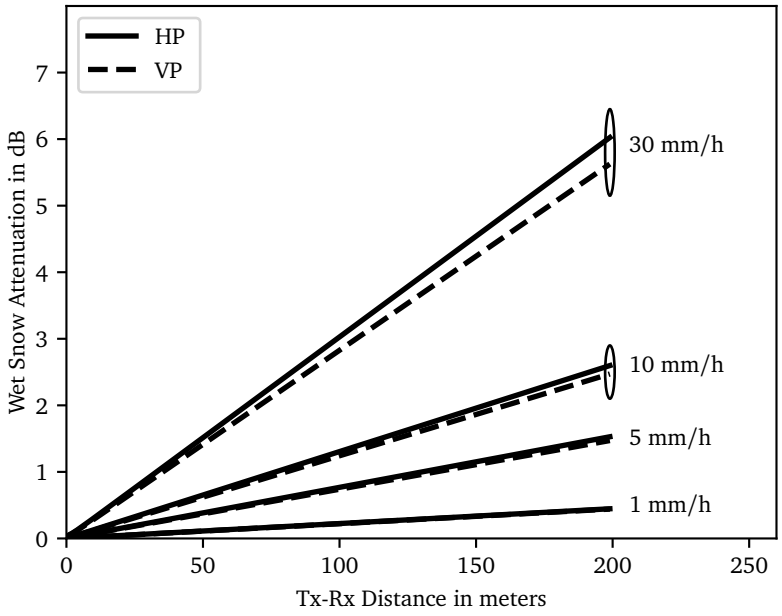

Figure 6.6 – Wet snow attenuation for different rain intensities, as a function of the communication distance ranging from 1 to 200 m.

The plot presents the estimated attenuation from combined rain and wet snow as a function of the communication distance ranging from 1 to 200 m for different rain intensities and two polarization types (horizontal and vertical). Since the method for estimating the attenuation from wet snow, uses as an input the estimated attenuation from rain, the results follow the same pattern as the attenuation results observed from rain. Similarly to the results presented for the rain, the attenuation from wet snow is a function of the rain intensity, communication distance, and polarization type.

As the rain intensity increases, the attenuation from the wet snow increases as well. Higher rain intensities are associated with larger drop sizes and a higher density of drops. As a result, the effect of the scattering and absorption is larger. At the same time, larger raindrops lead to a higher attenuation for the horizontal polarization compared to the vertical polarization, as depicted from the plot, due to the drop shape. Finally, as the communication distance increases, the attenuation increases proportionally. The influence of the communication distance is almost neglectable

for low intensity like 1 mm/h. On the other hand, as the intensity increases, like in the case of 30 mm/h, the attenuation increases rapidly with the transmission distance.

It is important to emphasize that the estimation of the attenuation from wet snow is done using the intensity values, extracted from the classification provided by the German Meteorological Service. The intensity of 30 mm/h is used in the simulations as a reference for maximum attenuation. Although the attenuation from wet snow is expected to be larger than the attenuation from rain, for the same intensity, since the intensities values for the wet snow are smaller than the intensity values considered for rain, reaching to 250 mm/h, I have decided to mostly inspect the impact of the rain in the the following sections, due to the stronger rates.

Yet to illustrate the larger impact of wet snow compared to pure rain, Figure 6.7 depicts the attenuation values estimated using the corresponding fading prediction methods, for the same rain intensity of 10 mm/h.

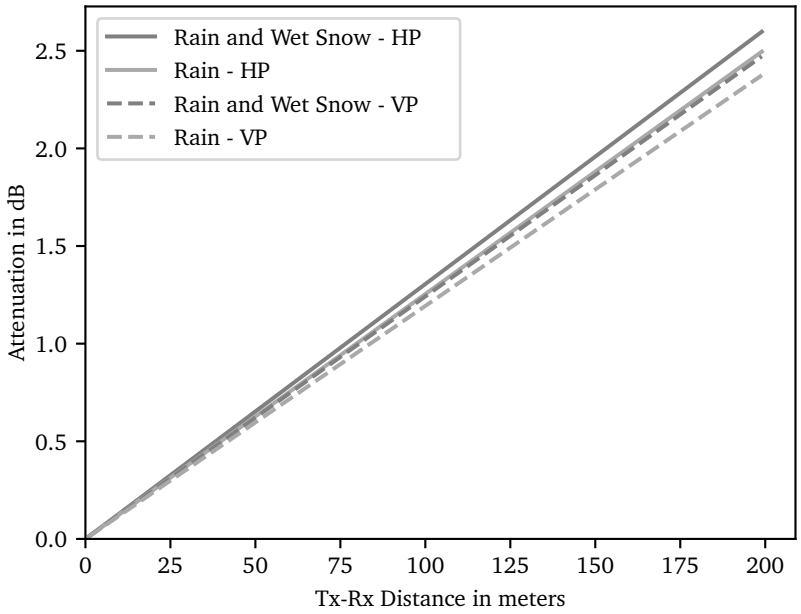

Figure 6.7 – Comparison between the attenuation from pure rain and wet snow, for vertical and horizontal polarization, as a function of the communication distance ranging from 1 to 200 m.

The simulations are conducted for the communication distance from 1 to 200 m, for horizontal and vertical polarizations. From the plot can be concluded that the attenuation from combined rain and wet snow is higher than the attenuation from pure rain for the same polarization type. This is a consequence of the particles in

the melting layer, covered by the thin layer of water, which attenuate the same as the particles were entirely water, but with a larger size.

The results of the wet snow attenuation and the comparison with the attenuation from rain, for long communication distances are given in Appendix B.1.

6.2.4 Path Loss

Each of the fading prediction methods is integrated into the channel model simulator, to investigate the impact of the rain and wet snow on the radio link. The attenuation estimated using the prediction methods is added in the decibel scale to the total path loss, computed by the channel model simulator using the CI free space reference distance model, described in Section 4.1.1.

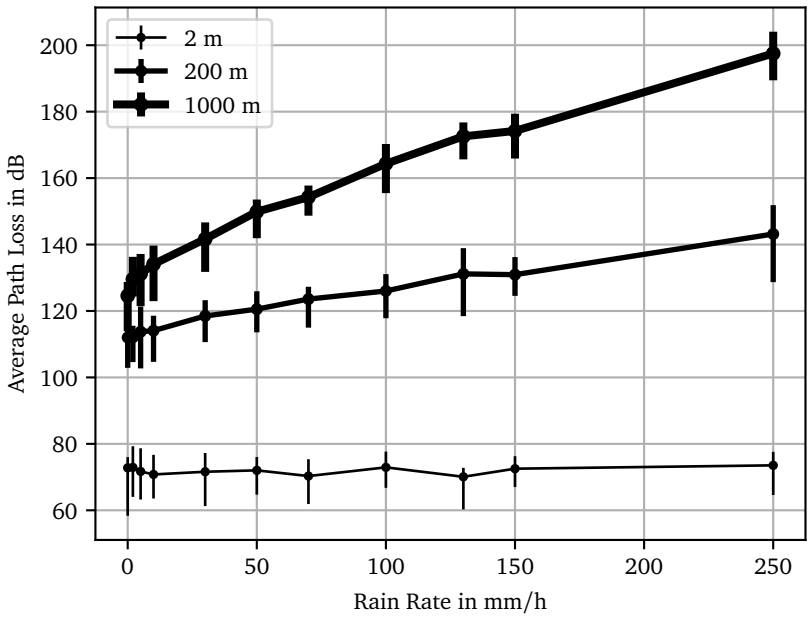

Figure 6.8 – The path loss results, for different fixed transmission distance, as a function of the rain intensity.

Since the simulator is a stochastic channel model, I have done several simulation repetitions and averaged the results for the path loss, and the PDP described in the following sections. The path loss values averaged over 15 simulation runs are shown in Figure 6.8 and are computed using the drop based model, for a static receiver in a fixed distance from the transmitter. The estimated path loss is given as a function of the rain intensity and only for the horizontal polarization, considering that it adds higher attenuation over the vertical polarization. The values are compared

for the communication distance of 2, 200 and 1000 m. Since the path loss value is computed in dB after each simulation run, the average value is estimated in the linear scale and converted to dB. Hence to understand the variation of the values, the 1 and 99 percentile is shown in the plot along with the mean.

Similarly to the conclusions derived from the rain attenuation results, the path loss plot depicts as well that for very small distances between the transmitter and receiver, for example, 2 m, the influence of rain is very small even for very strong intensities like 250 mm/h. Yet when the transmission distance increases, the impact from the rain is small for light and moderate rain, but it starts increasing at strong rainfalls. The path loss results when wet snow is present are given in Appendix B.2.

6.2.5 Power Delay Profile

Besides the path loss, the PDP is another metric generated by the simulator. The results for the PDP are shown in Figure 6.9 for a transmission distance of 2 m and in Figure 6.10 for a transmission distance of 200 m. The results for the distance 1000 m are shown in Appendix A.2. For each distance, the results are presented for the rain intensity 10 and 100 mm/h. To average the results over 15 simulation runs, as was previously mentioned, the number of time clusters has been fixed to 6. The plots show only the subpath components having the received power higher than a specific threshold. The value of the threshold is calculated by the difference between the transmitted power and the dynamic range, defined by the simulator as the maximum omnidirectional path loss. The values used for the dynamic range are the ones recommended by the simulator. Based on the transmitted power defined in Table 6.7, for distances smaller than 500 m the threshold is -205 dBm, while for distances larger than 500 m the threshold is -175 dBm.

The conclusions derived from the plots can be in terms of the power and the propagation delay.

For the transmission distance of 2 m, the influence of rain in the receiver power is very small, independently of the rain intensity. The received power for each subpath component when the rain intensity is 10 mm/h is similar to the case when the intensity is 100 mm/h as it can seen in Figure 6.9 a and b. Once the transmission distance increases to 200 m, the intensity of rain plays an important role in the attenuation of the signal, as it can be seen from the level of the received power in Figure 6.10 a and b. For the same rain intensity but for different transmission distance, it can be seen that the level of the received power rapidly decreases, reducing at the same time, the number of the subpath components reaching the receiver.

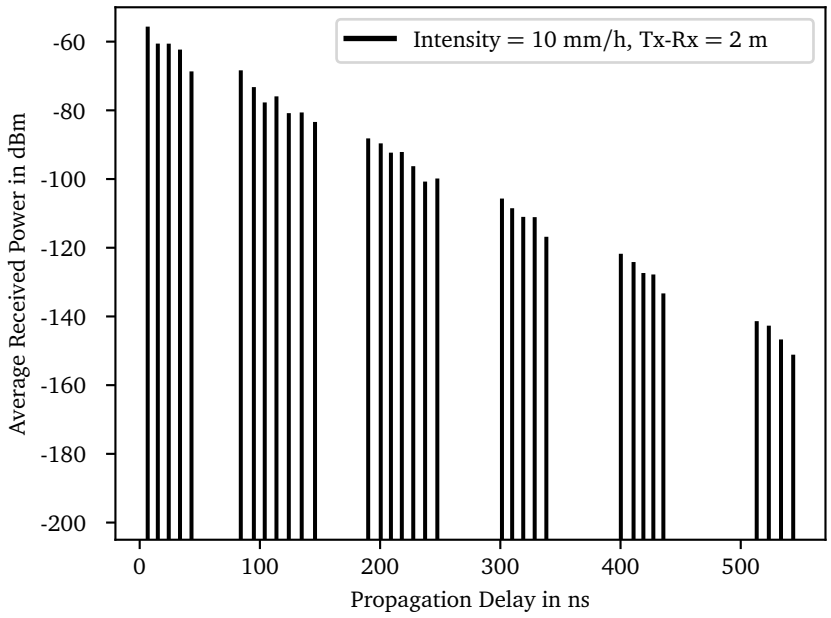

(a) PDP 10 mm/h

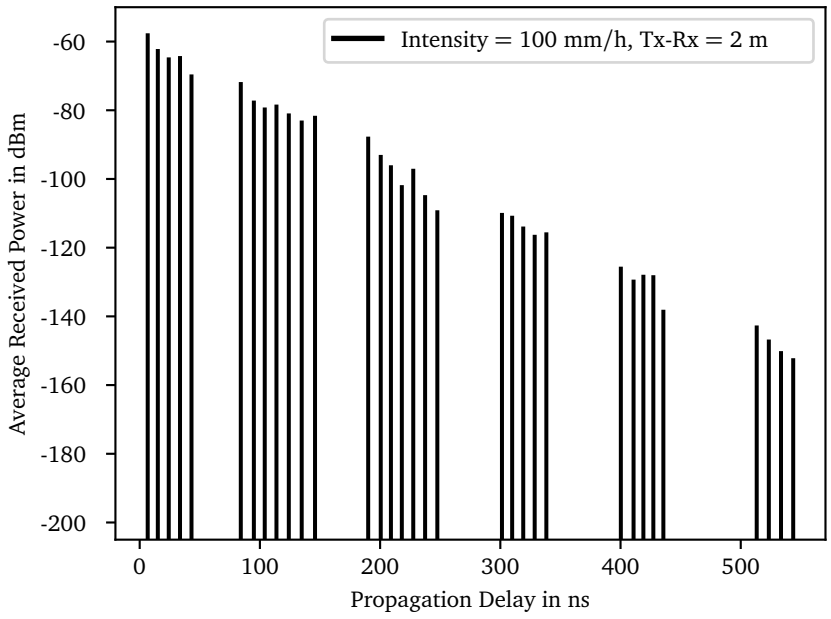

(b) PDP 100 mm/h

Figure 6.9 – PDP for transmission distance 2 m.

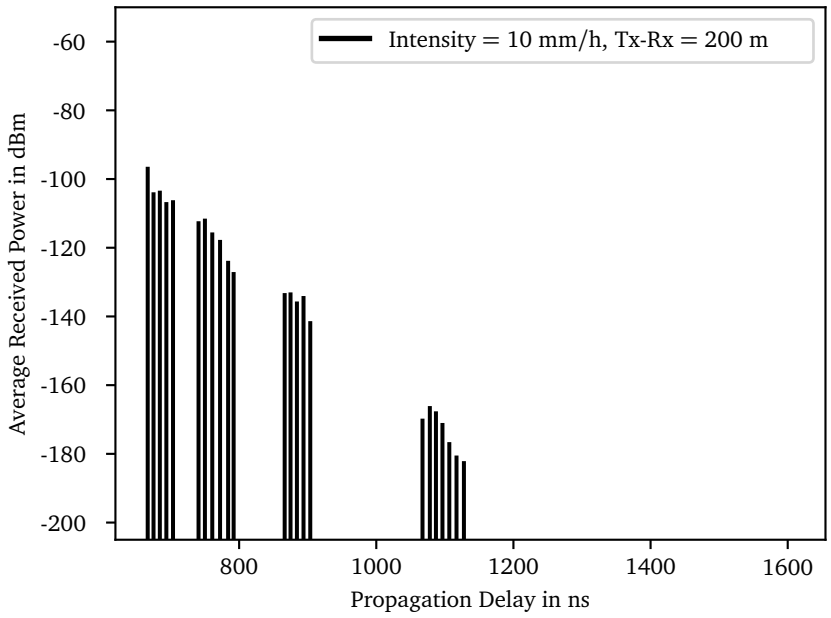

(a) PDP 10 mm/h

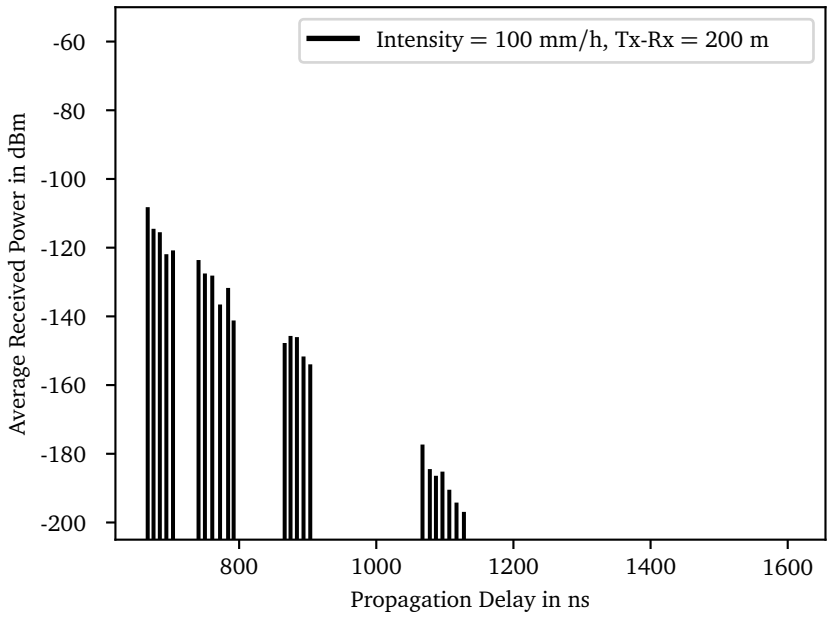

(b) PDP 100 mm/h

Figure 6.10 – PDP for transmission distance 200 m.

The other conclusion that can be extracted from this scenario is in terms of the propagation delay. Since the distance between the transmitter and the receiver increases, the time at which the first subpath component will reach the destination is different. In the case when the distance is 2 m, the first subpath component will reach the destination after approximately 6.7 ns, but as the distance increases to 200 m, the first subpath components reach the destination after approximately 670 ns. As a consequence of longer propagation paths, the received power of the subpath components reaching the receiver will be lower. To better understand this behavior, Figure 6.11 shows the PDP computed by the spatial consistency model, for the receiver moving from the distance 1 to 200 m away from the transmitter. The polarization is horizontal and the rain intensity is 100 mm/h. The plot depicts that as the receiver moves further away from the transmitter, the propagation delay or the time when the first subpath component reaches the destination increases aswell. Furthermore, with the distance increasing, the power of the first subpath component decreases. As a consequence of the power decreasing, the number of clusters reaching the destination decreases, for example from 6 when the distance is 2 m, to 4 when the distance approaches 200 m.

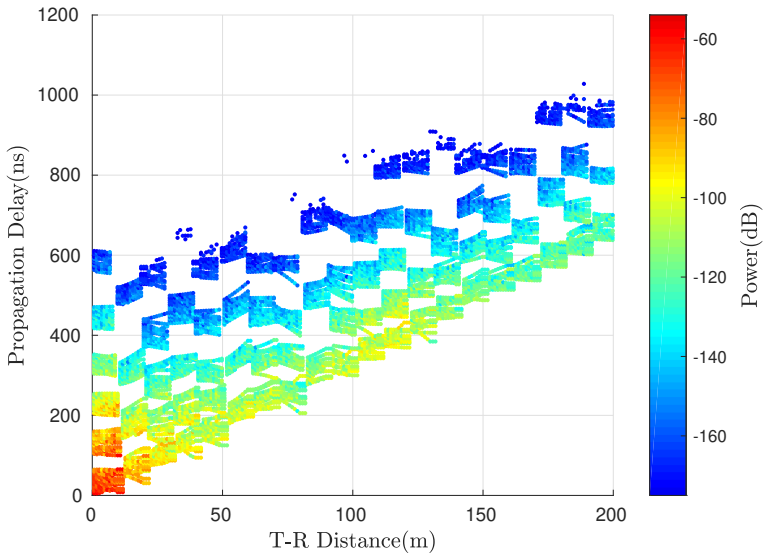

Figure 6.11 – The PDP results, generated by the spatial consistency model, for the horizontal polarization and rain intensity 100 mm/h.

Another characteristic of the plot related to the structure of the simulator is the pattern of the results organized in blocks. This behavior is a consequence of the correlation distance for shadow fading, leading to a receiver experiencing a similar scattering environment during mobility. But in these blocks, it is spotted an issue. As the distance between the transmitter and receiver increases, in some cases,

the first subpath component comes earlier than some other subpath components corresponding to lower distances. This issue has been spotted in different parts of the plot. One possible explanation is that the results are given in Figure 6.11, are collected from only one simulation run and this behavior might be a consequence of the fact that the simulator is a stochastic channel model.

Chapter 7

Conclusion

In this thesis, I investigated the impact of rain and wet snow on the radio links at 60 GHz, using the NYUSIM. For estimating the attenuation from the aforementioned weather variations, I have selected the rain fading prediction method described in ITU-R P. 530-17, and the combined method for rain and wet snow described in ITU-R P. 530-15. The fading prediction methods are implemented in MATLAB and then are integrated into the NYUSIM, in order to study the impact of weather variations on the radio links.

The simulator provides a function for computing the attenuation from the atmospheric variations, including rain. In order to investigate the difference between the simulator method and the implemented method, the attenuation from rain is computed for different intensities and communication distances, using these models. The results, for the communication distance ranging from 1–200 m, have shown that the values computed using the implemented prediction method are larger compared to the results estimated by the simulator method. The difference between the results gets larger for strong rain intensities and communication distance. In addition, the simulator method, differently from the implemented method, does not consider the polarization type as a factor influencing the attenuation results. But, considering the drop shape and the fact that in 60 GHz the length of the wave is comparable with the drop diameter, the polarization type is a parameter influencing the attenuation. As a result, the simulator method has been replaced by the implemented method.

Furthermore, the atmospheric attenuation, capturing the effect of dry air (including O_2), water vapor (H_2O), rain and haze, is computed using real data for the temperature, humidity, barometric pressure, and rain intensity, collected from the weather station at Paderborn University. The computation is done using the function provided by the simulator for the estimation of the atmospheric attenuation without the component of rain, adding afterward the rain attenuation computed using the fading prediction method. For the considered scenarios and the communication

distance ranging from 1–200 m, the atmospheric attenuation reached small values. However, the attenuation depends on parameters (temperature, humidity, etc,) that take different values based on the weather conditions and is computed only for three scenarios where the rain intensity was small.

In order to explore the impact of the weather variations on signal propagation, I ran multiple simulations, considering as a scenario the communication between two vehicles. The analysis were focused on short communication distances, yet the behavior of some metrics have been analyzed for long distances as well.

The results have shown that the rain attenuation and the attenuation from the wet snow, increases as the rain intensity and the communication distance increases. At very short transmission distances, the attenuation from rain and wet snow have shown to reach small values, even for strong rainfalls. At long communication distances, the attenuation reached again small values for ligh and moderate intensities and it increased rapidly for strong intensities. As expected, polarization was another factor influencing the attenuation. Due to the drop shape, the attenuation for the horizontal polarization was higher compared to the vertical polarization. The difference was more visible for strong rain intensities and large communication distance.

Secondly, the results have shown that for the same scenario, in Paderborn, the attenuation from wet snow reached higher values compared to attenuation from rain. This is a consequence of the particles in the melting layer attenuating as they were entirely water, but with larger sizes.

These results demonstrate that the influence of the weather variations (specifically rain and wet snow) on signal attenuation at 60 GHz is almost negligible at very short communication distances. This influence becomes crucial for long communication distances and especially strong rainfalls.

7.1 Future Work

The results presented in this thesis give an insight into the impact of rain and wet snow on signal attenuation at 60 GHz. The method used for estimating the attenuation from wet snow was the combined method for rain and wet snow described in ITU-R P. 530-15. As previously mentioned, this method was changed in the latest standard version ITU-R P. 530-17. A comparison of the results from these two models for different locations might be intersting to investigate. Furthermore, the attenuation results from the wet snow, presented in the thesis, are computed only for one specific location, which is Paderborn. The impact of the wet snow could be also studied for other scenarios, with different altitudes and mean rain height.

Even though in different works it is mentioned that the impact of the dry snow in signal attenuation is negligible, the investigation of the attenuation values and a comparison with the ones from estimated from the wet snow might be interesting.

Also, the comparison between the implemented rain fading prediction method and the simulator method might be interesting the investigate for long communication distances as well. Furthermore, the total atmospheric attenuation can also be explored for other scenarios using real data for the temperature, barometric pressure, humidity, and rain intensity.

List of Abbreviations

3GPP	3rd Generation Partnership Project
AoA	Angle of Arrival
AoD	Angle of Departure
APDP	Average Power Delay Profile
CI	Close-in
CIR	Channel Impulse Responses
DS	Delay Spread
DSD	Rain Drop Size Distribution
FSPL	Free space path loss
HPBW	Half Power Beamwidth
ITU	International Telecommunication Union
ITU-R	International Telecommunication Union-Radiocommunication
LOS	Line of Sight
LS	least square
METIS	Mobile and wireless communications Enablers for the Twenty-twenty Information Society
MiWEBA	Millimeter-Wave Evolution for Backhaul and Access
mmWave	Millimeter Wave
MPC	Multi Path Component
NLOS	Non Line of Sight
OFDM	Orthogonal Frequency Division Multiplex
PDP	Power Delay Profile
PLE	Path loss exponent
QuaDRiGa	QUAsi Deterministic RadIo channel GenerAtor
RT	Ray Tracing
SF	shadow fading standard deviation

SL	Spatial Lobe
SSCM	Statistical Spatial Channel Model
TC	Time Cluster
UMi	Urban Microcell

List of Figures

List of Tables

Bibliography

[1] X. Wang, L. Kong, F. Kong, F. Qiu, M. Xia, S. Arnon, and G. Chen, "Millimeter wave communication: A comprehensive survey," *IEEE Communications Surveys & Tutorials*, vol. 20, no. 3, pp. 1616–1653, 2018.

[2] I. A. Hemadeh, K. Satyanarayana, M. El-Hajjar, and L. Hanzo, "Millimeter-wave communications: Physical channel models, design considerations, antenna constructions, and link-budget," *IEEE Communications Surveys & Tutorials*, vol. 20, no. 2, pp. 870–913, 2017.

[3] M. C. Kestwal, S. Joshi, and L. S. Garia, "Prediction of rain attenuation and impact of rain in wave propagation at microwave frequency for tropical region (Uttarakhand, India)," *International Journal of Microwave Science and Technology*, vol. 2014, 2014.

[4] I. Shayea, T. A. Rahman, M. H. Azmi, and M. R. Islam, "Real Measurement Study for Rain Rate and Rain Attenuation Conducted Over 26 GHz Microwave 5G Link System in Malaysia," *IEEE Access*, vol. 6, pp. 19 044–19 064, May 2018. DOI: 10.1109/ACCESS.2018.2810855.

[5] S. Shrestha and D.-Y. Choi, "Rain attenuation statistics over millimeter wave bands in South Korea," *Journal of Atmospheric and Solar-Terrestrial Physics*, vol. 152, pp. 1–10, 2017.

[6] T. Tjelta and D. Bacon, "Predicting combined rain and wet snow attenuation on terrestrial links," *IEEE Transactions on Antennas and Propagation*, vol. 58, no. 5, pp. 1677–1682, 2010.

[7] L. Raschkowski, P. Kyösti, K. Kusume, T. Jämsä, V. Nurmela, A. Karttunen, A. Roivainen, T. Imai, J. Järveläinen, J. Medbo, et al., "METIS Channel Models," Mobile and wireless communications Enablers for Twenty-twenty, Technical Report ICT-317669-METIS/D1.4, Jul. 2015.

[8] R. J. Weiler, M. Peter, W. Keusgen, A. Maltsev, I. Karls, A. Pudeyev, I. Bolotin, I. Siaud, and A.-M. Ulmer-Moll, "Quasi-deterministic millimeter-wave channel models in MiWEBA," *EURASIP Journal on Wireless Communications and Networking*, vol. 2016, no. 1, p. 84, 2016.

[9] S. Jaeckel, L. Raschkowsk, K. Börner, L. Thiele, F. Burkhardt, and E. Eberlein, "QuaDRiGa- Quasi Deterministic Radio Channel Generator, User Manual and Documentation," Fraunhofer Heinrich Hertz Institute, Technical Report v2.0.0, Aug. 2017.

[10] S. Sun, G. R. MacCartney, and T. S. Rappaport, "A novel millimeter-wave channel simulator and applications for 5G wireless communications," in *IEEE International Conference on Communications (ICC) 2017*, Paris, France, May 2017. DOI: 10.1109/ICC.2017.7996792.

[11] D. M. Matic, H. Harada, and R. Prasad, "Indoor and outdoor frequency measurements for MM-waves in the range of 60 GHz," in *48th IEEE Vehicular Technology Conference (VTC'98)*, Ottawa, Canada, May 1998. DOI: 10.1109/VETEC.1998.686638.

[12] M. Peter, R. Weiler, B. Göktepe, W. Keusgen, and K. Sakaguchi, "Channel measurement and modeling for 5G urban microcellular scenarios," *MDPI Sensors*, vol. 16, no. 8, p. 1330, 2016.

[13] R. J. Weiler, M. Peter, W. Keusgen, and M. Wisotzki, "Measuring the busy urban 60 GHz outdoor access radio channel," in *IEEE International Conference on Ultra-WideBand (ICUWB)*, Paris, France, Sep. 2014. DOI: 10.1109/ICUWB.2014.6958971.

[14] S. Ju, S. Sun, and T. S. Rappaport, "NYUSIM User Manual," New York University and NYU WIRELESS, User Manual v. 2.0, Sep. 2019.

[15] P. Kántor, J. Bitó, and Á. Drozdy, "Characteristics of 5G wireless millimeter wave propagation: Transformation of rain attenuation applying different prediction models," in *10th European Conference on Antennas and Propagation (EuCAP 2016)*, Davos, Switzerland, Apr. 2016. DOI: 10.1109/EuCAP.2016.7481358.

[16] P. Thorvaldsen, C. H. Bernhoft, and I. Henne, "Outdoor transmission measurement at 26 GHz; Results of a 3 years trial in Norway," in *10th European Conference on Antennas and Propagation (EuCAP 2016)*, Davos, Switzerland, Apr. 2016. DOI: 10.1109/EuCAP.2016.7481363.

[17] P. Thorvaldsen and I. Henne, "Propagation measurements on a line-of-sight over-water radio link in Norway," *Radio Science*, vol. 49, no. 7, pp. 531–548, 2014.

[18] International Telecommunication Union, "Propagation data and prediction methods required for the design of terrestrial line-of-sight systems," ITU-R, Recommendation P.530-15, Sep. 2013.

[19] J. S. Seybold, Introduction to RF propagation. John Wiley & Sons, 2005.

[20] International Telecommunication Union, "Propagation data and prediction methods required for the designof terrestrial line-of-sight systems," ITU-R, Recommendation P.530-17, Dec. 2017.

[21] T. Teshirogi, Modern millimeter-wave technologies. Ios Press, 2001.

[22] C. D. Ahrens, Essentials of meteorology: an invitation to the atmosphere. Cengage Learning, 2011.

[23] S. Sun, T. S. Rappaport, T. A. Thomas, A. Ghosh, H. C. Nguyen, I. Z. Kovács, I. Rodriguez, O. Koymen, and A. Partyka, "Investigation of prediction accuracy, sensitivity, and parameter stability of large-scale propagation path loss models for 5G wireless communications," *IEEE Transactions on Vehicular Technology*, vol. 65, no. 5, pp. 2843–2860, May 2016.

[24] M. K. Samimi and T. S. Rappaport, "3-D millimeter-wave statistical channel model for 5G wireless system design," *IEEE Transactions on Microwave Theory and Techniques*, vol. 64, no. 7, pp. 2207–2225, 2016.

[25] S. Ju and T. S. Rappaport, "Millimeter-Wave Extended NYUSIM Channel Model for Spatial Consistency," in *IEEE Global Communications Conference (GLOBECOM 2018)*, Abu Dhabi, United Arab Emirates, Dec. 2018.

[26] S. Ju and T. S. Rappaport, "Simulating Motion - Incorporating Spatial Consistency into NYUSIM Channel Model," in *88th IEEE Vehicular Technology Conference (VTC2018-Fall)*, Chigaco, IL, Aug. 2018.

[27] R. J. Weiler, M. Peter, W. Keusgen, H. Shimodaira, K. T. Gia, and K. Sakaguchi, "Outdoor millimeter-wave access for heterogeneous networks — Path loss and system performance," in *25th IEEE Annual International Symposium on Personal, Indoor, and Mobile Radio Communication (PIMRC 2014)*, Washington, D.C., Sep. 2014.

[28] International Telecommunication Union, "Specific attenuation model for rain for use in prediction methods," ITU-R, Recommendation P.838-3, Mar. 2005, pp. 1–8.

[29] ——, "Characteristics of precipitation for propagation modelling," ITU-R, Recommendation P.837-7, Jun. 2017.

[30] D. A. de Wolf, "On the Laws-Parsons distribution of raindrop sizes," *Radio Science*, vol. 36, no. 4, pp. 639–642, 2001.

[31] A. Maitra, "Rain attenuation modeling from measurements of rain drop size distribution in the Indian region," *IEEE Antennas and Wireless Propagation Letters*, vol. 3, no. 1, pp. 180–181, 2004.

[32] International Telecommunication Union, "Rain height model for prediction methods," ITU-R, Recommendation P.839-4, Sep. 2013.

[33] T. S. Rappaport, R. W. Heath Jr, R. C. Daniels, and J. N. Murdock, Millimeter wave wireless communications. Pearson Education, 2015.

[34] R. Stull, Practical Meteorology: An Algebra-based Survey of Atmospheric Science. Vancouver, Canada: UBC Press, 2015.

[35] H. J. Liebe, G. A. Hufford, and M. G. Cotton, "Propagation modeling of moist air and suspended water/ice particles at frequencies below 1000 GHz," in *AGARD Electromagnetic Wave Propagation Panel Symposium*, Palma de Mallorca, Spain, May 1993, pp. 3.1–3.10.

Appendices

Appendix A

Rain attenuation for long distances

A.1 Rain Attenuation

As explained in Section 6.2.2, the rain attenuation represents the total attenuation from the presence of rain in the transmission medium. The simulation results are given in Figure A.1 and show the rain attenuation in decibel as a function of the communication distance ranging from 1 to 1000 m.

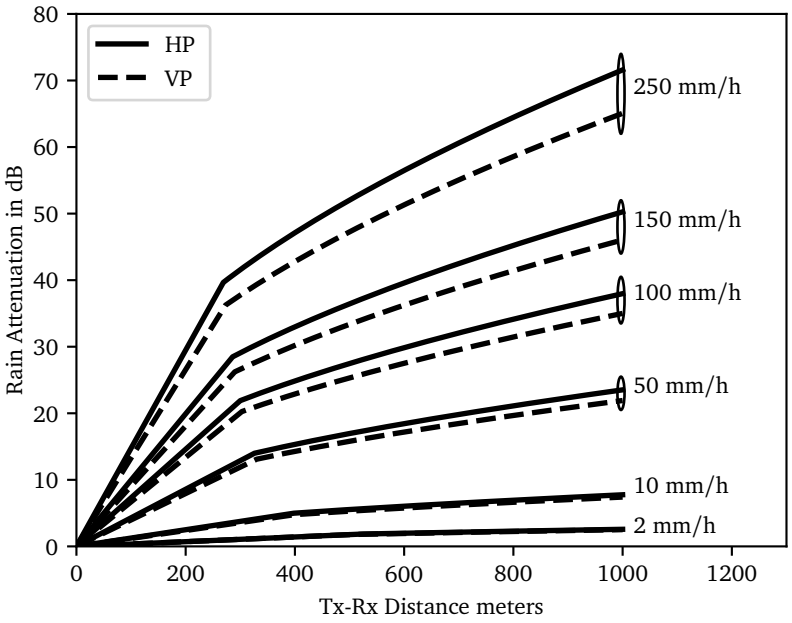

Figure A.1 – Rain attenuation for different rain intensities, as a function of the distance between the transmitter and receiver ranging from 1 to 1000 m.

The simulations are done for the rain intensities given in Table 6.3 and for the horizontal and vertical polarization. The results depicted in Figure A.1 show that the impact of light and moderate rain in the signal attenuation is small even at very long communication distances. The attenuation increases rapidly for strong rain intensities, reaching values of approximately 70 dB for horizontal polarization and transmission distance of 1 km.

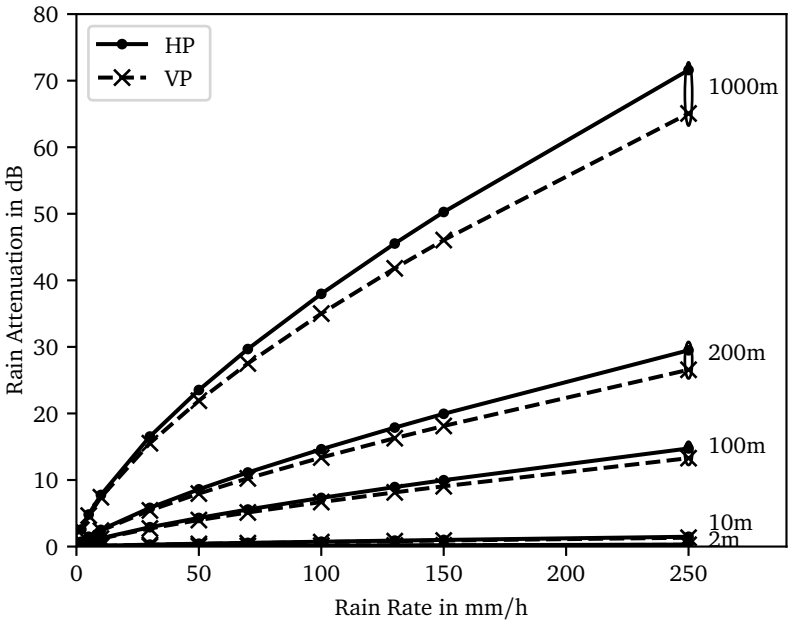

Figure A.2 – Rain attenuation for different fixed distances between the transmitter and receiver, as a function of the rain intensity.

The factor of polarization plays an important role only for very strong rain intensities where the difference between the attenuation from the two types of polarization reaches the value of almost 10 dB. Differently from the plot shown in Figure 6.3 of Section 6.2.2, which gives the rain attenuation but as a function of the communication distance ranging from 1 to 200 m, in this plot, the slope of the lines changes. The slop of the plot changes at a specific point of the transmission distance, which is different for given rain intensities. This behavior is not present for light and moderate rain but is starts being visible only at strong rain intensities. This is a result of the distance factor given in Equation 5.3 of Section 5.1.1. As described in Section 5.1.1, according to ITU-R P. 530-17 [20], the maximum value of the distance vector should be 2.5. In the cases when the value of the denominator is smaller than 0.4, the value of the distance factor is 2.5. The point in the plot where the line changes the slop corresponds to the value for which the denominator gets larger than 0.4.

Another way for exploring the attenuation from rain is as a function of different rain intensities but for fixed communication distance as Shown in Figure A.2. The plot illustrates again the importance of the communication distance. For short transmission distance in the range of 10 m, the total attenuation from rain, including the scenario for a very strong intensity, is limited. At the same time, the effect of the polarization is almost unnoticeable, even at the intensity of 250 mm/h.

A.2 Power Delay Profile

The PDP is computed for the transmission distance of 1000 m for two different rain intesities, 10 and 100 mm/h. The simulations are conducted using the configuration setup for the drop based model given in Table 6.7 and the results are presented in Figure A.3 considering only the horizontal polarization. The results are averaged over 15 simulation runs. From the plot, it can be observed that the first subpath component reaches the receiver after 3333 ns. Due to the very long propagation path, the received power of the first subpath component, coming from the LOS link, is in the order of −120 dBm for the rain intensity of 10 mm/h and it decreases to almost −150 dBm as the rain intensity increases to 100 mm/h. Another conclusion related to the received power is the number of clusters. It is important to reemphasize that this number has been fixed to 6 for all the simulations. The subpath components shown in the plots are only the ones having a receiver power higher than the value of the threshold −175 dBm. Hence the plots depict that the number of clusters reaching the receiver decreases to 4 for the rain intensity of 10 mm/h, and as the intensity is increased, the number of the clusters decreases at 2.

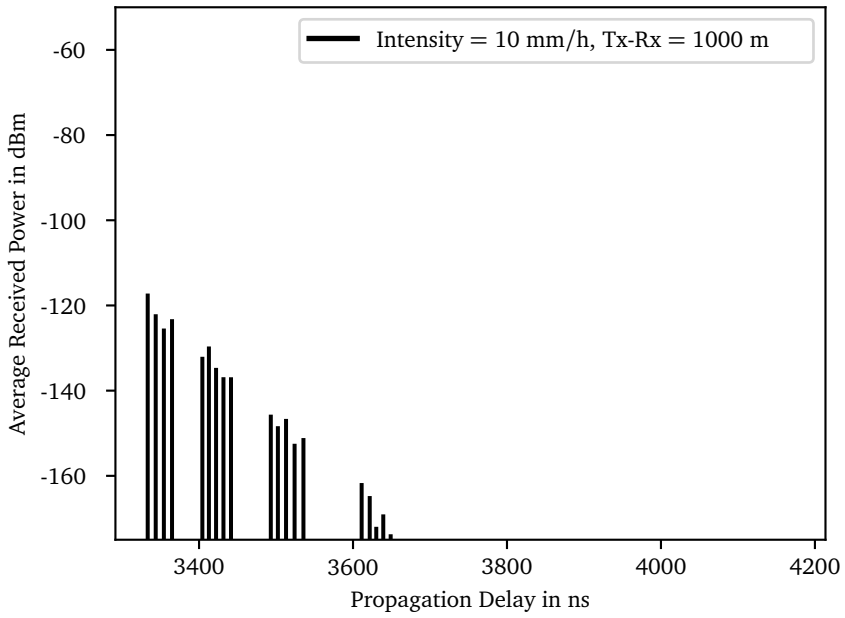

(a) PDP 10 mm/h

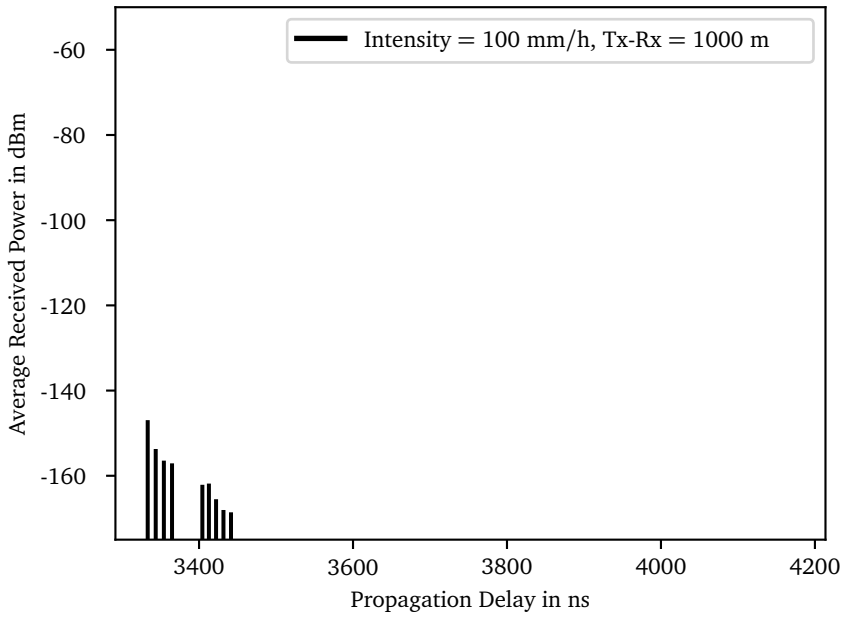

(b) PDP 100 mm/h

Figure A.3 – The PDP results for transmission distance 1000 m.

Appendix B

Wet Snow Attenuation for long distances

B.1 Wet Snow Attenuation

Similarly to the case of rain, the attenuation from combined rain and wet snow is also analyzed for long communication distances.

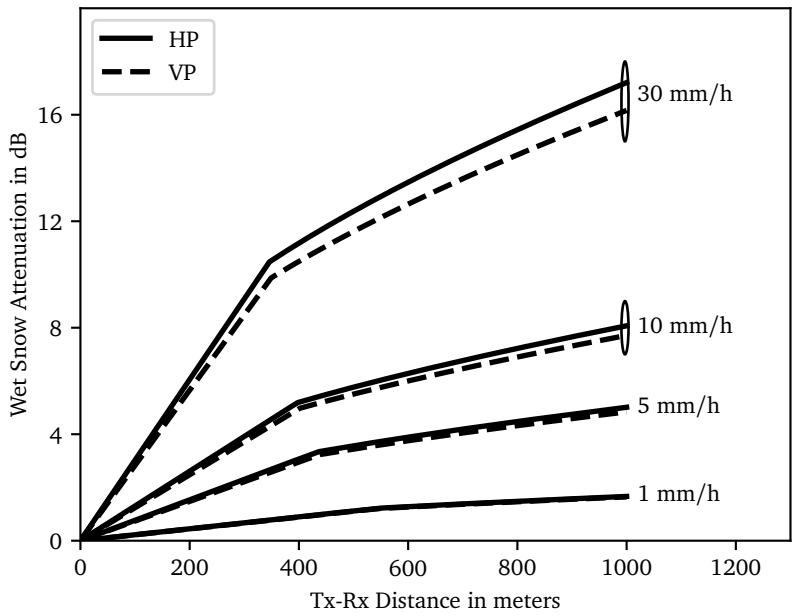

Figure B.1 – Wet snow attenuation for different rain intensities, as a function of the communication distance ranging from 1 to 1000 m.

Figure B.1 shows the value of the attenuation from combined rain and wet snow estimated using the fading prediction method, for different rain intensities and polarization types, as a function of the transmission distance from 1 to 1000 m.

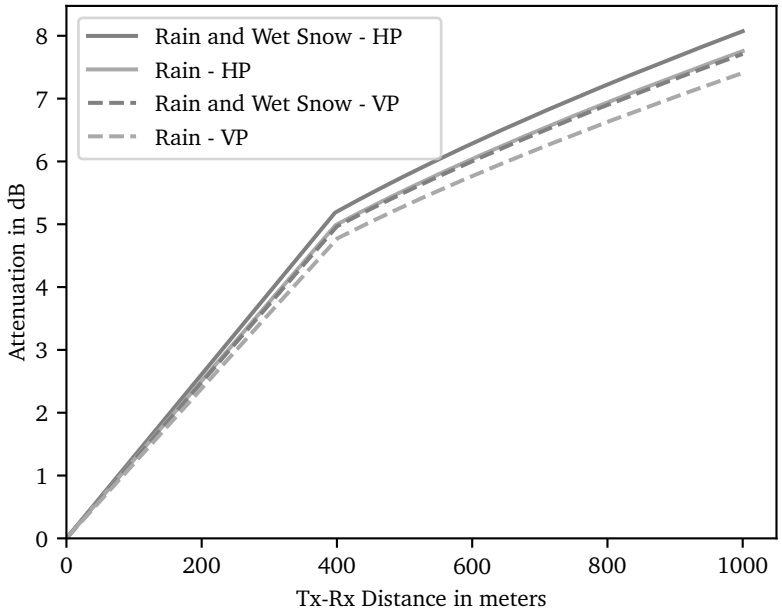

Figure B.2 – Comparison between the attenuation from pure rain and combined rain and wet snow, for vertical and horizontal polarization, as a function of the communication distance ranging from 1 to 1000 meters.

Considering that the combined fading prediction method for estimating the attenuation from rain and wet snow uses as input the attenuation from rain, estimated using the rain fading prediction method, the results follow the same behavior as the one shown in Figure A.1. The attenuation value and the difference between the two polarization types increase along with the rain intensity. This attenuation is very small for light and moderate intensities even at the distance of 1000 m, and it increases rapidly with the intensity. As described in Section A.1, the lines change the slope due to the distance factor, at the point where the distance factor gets value smaller than 2.5.

Since the generated plot has a similar pattern to the one computed from the rain attenuation, it might be interesting to observe the difference between these results. Figure 6.7 compares the attenuation from rain and wet snow for the two polarization types and the intensity 10 mm/h. The plot shows that for the same polarization, the attenuation from combined rain and wet snow is larger compared to the attenuation from rain. This is a consequence of the ice drops covered by the

thin layer of water, which attenuates the same as the drop was entirely water, but with a larger size. As was expected the difference between the two attenuations increases for longer transmission distances.

B.2 Path Loss

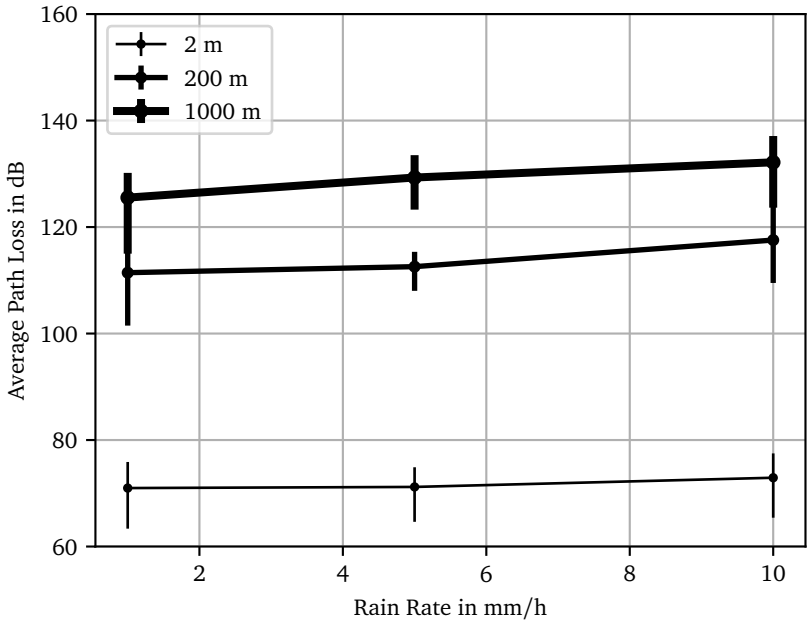

Figure B.3 – Path loss results from the wet snow, for different fixed distances, as a function of the rain intensity.

Similarly to Figure 6.8, the path loss is also computed for the case when wet snow is present in the transmission medium. The attenuation from wet snow is added in decibel to the total path loss computed by the NYUSIM without considering the term for the atmospheric attenuations. The results for the path loss averaged over 15 simulation runs as a function of the rain intensity are given in Figure B.3. The simulations are done using the drop based model, for a static receiver and only for horizontal polarization. Along with the average value for each intensity, the 1 and 99 percentile have been also computed. The plot depicts that the contribution of the wet snow attenuation is almost negligible at very small intensities. This influence starts increasing only at a very long transmission distance as 1 km.

Appendix C

Regression Coefficient Values

Table C.1 lists the regression coefficient values for the horizontal and vertical polarization, used for the validation of the rain fading prediction method.

Table C.1 – Regression coefficient values for different frequencies for estimating the specific rain attenuation based on the ITU-R P. 838-3 [28].

Frequency (GHz)	k_H	α_H	k_V	α_V
1	0.0000259	0.9691	0.0000308	0.8592
10	0.01217	1.2571	0.01129	1.2156
23	0.1286	1.0214	0.1284	0.9630
30	0.2403	0.9485	0.2291	0.9129
38	0.4001	0.8816	0.3844	0.8552
40	0.4431	0.8673	0.4274	0.8421
60	0.8606	0.7656	0.8515	0.7486
70	1.0315	0.7345	1.0253	0.7215
90	1.2807	0.6944	1.2795	0.6876
100	1.3671	0.6815	1.3680	0.6765
200	1.6378	0.6382	1.6443	0.6343
300	1.6286	0.6296	1.6286	0.6262
400	1.5860	0.6262	1.5820	0.6256
500	1.5418	0.6253	1.5366	0.6272
600	1.5013	0.6262	1.4967	0.6293
700	1.4654	0.6284	1.4622	0.6315
800	1.4335	0.6315	1.4321	0.6334
900	1.4050	0.6353	1.4056	0.6351
1000	1.3795	0.6396	1.3822	0.6365